KATHOLIEKE UNIVERSITEIT
LEUVEN

Faculteit
Ingenieurswetenschappen

Synaptoprobe

Interfacing at the synapse level

Jasper Timmerman

Thesis submitted to
obtain the degree of Master
in Engineering:
nanotechnology,
with an option in bionanotechnology

Promotor:
Prof Dr Marc Heyns

Assessor:
Prof Dr Joris De Wit
Prof Dr Sebastian Haesler

Daily supervisor:
Luis Diego Hoffman
Prof Dr Jennifer Patterson

Academic Year 2016 - 2017

Foreword

How fitting that I am sat here behind my desk on a Sunday afternoon to write these last words in completion of my (second) master's thesis. Before I can reflect upon the experiences I had and the lessons I have learned throughout this year, there are so many people I want to thank from the bottom of my heart first.

Professor Heyns, who was the one to accept me into the nano program in the first place, for allowing me to follow my heart and my head that in unison drove me to Nerf.

Professor Haesler for giving me the chance to take this project and make it my own. And all the people at Nerf for creating an amazing environment to do high quality science in a positive and constructive way. Thank you to Martijn and Horacio, for putting up with me. And especially a big thank you to the real MVP Luis Diego 'Jupon' Hoffman, always an engineer, always a tutor, always a friend.

Professor Patterson and everyone at the biomaterials group who made me feel so welcome as a part of the group, and have helped me out countless times with indispensable advice, and always with a smile.

And to all the people that have contributed in all the myriad ways big and small to this project, I thank you for being who you are and doing what you do.

This year has been an amazing ride. The thing about personal growth is that you don't know you're doing it until you look back and see a different person than you expected to see. Makes me think about the person in the future. I hope he looks back every now and then, I will wave back sometime.

OK

Jasper

Table of Contents

Abstract

The field of brain machine interfacing and neuroscience in general is rapidly expanding. Exciting new technologies are being developed for the near future. To expedite the developments in neuroscience and brain machine interfacing the development of a novel concept probe is explored. The synaptoprobe is designed to make specific connections with targeted subpopulations of neurons. Conceptually the synaptoprobe would utilize the unique properties of synaptogenic proteins immobilized onto electrode surfaces. In the approach described here, a conductive hydrogel is deposited onto electrodes as a scaffold for synaptogenic proteins neuroligin 1 and LRRTM 2, while maintaining low impedance and improving biocompatibility. The synthesis of the hydrogel was achieved, and two different pathways to immobilize neuroligin 1 and LRRTM 2 were developed.

List of figures and tables

List of figures

List of tables

List of abbreviations and symbols

µCP	microcontact printing
11-BUDA	11-bromodecanoic acid
AChE	Acetylcholinesterase
AP	Action potential
Au	Gold
Bsn	Bassoon
Ca+	Calcium ion
CHG	Conductive hydrogel
CNS	Central nervous system
CP	Conductive polymer
DAPI	4',6-diamidino-2-phenylindole
ECM	Extracellular matrix
EDC	1-ethyl-3-(-3-dimethylaminopropyl) carbodiimide
FGF	Fibroblast growth factor
GMA	Glycidyl methacrylate
IPN	Interpenetrated network
ITO	Indium Tin Oxide
K+	Potassium ion
LRRTM2	Leucine rich repeating transmembrane protein 2
MA	Methacrylic anhydrate
MAP-2	Microtubule associated protein-2
MEA	Multi electrode array
MES	2-(N-morpholino)ethanesulfonic acid
MFI	Mean fluorescence intensity
MFI	Mean fluorescent intensity
Na+	Sodium ion
NaOH	Sodium hydroxide
NCAM	Neural cell adhesive molecule
NGF	Neural growth factor
NHS	N-hydroxysuccinimide
NLGN1	Neuroligin-1
NMR	Nuclear Magnetic resonance
PANI	Poly aniline
PBS	Phosphate buffered saline

PCB	Printed circuit board
PDK	Poly-D-lysin
PDMS	Polydimethylsiloxane
PEDOT	Poly-(3,4-ethylenedioxy)thiophene
PLL	Poly-L-Lysine
PNS	Peripheral nervous system
PPY	Poly pyrrole
PSS	Poly styrene sulfonate
PT	Poly thiophene
Pt	Platinum
PTs	Para toluene sulfonate
PVA	Poly vinyl alcohol
SEM	Scanning electron microscopy
SLB	Suspended Lipid Bilayer
TiN	Titanium nitride

Chapter 1: Introduction

The human brain is the most complex biological system known to mankind. The structural and functional properties of the grey and white matter of the brain is what allows humans to decode the symbols of this text for example, and to interpret them to derive meaning. That is the result of millions of years of evolution through natural selection. The successes of *Homo sapiens* have largely been attributed to their ingenuity, which finds its foundation in the development of the neocortex of the brain brought on by natural selection.[1, 2] The development of the neocortex has allowed hominids to develop language and to use logic to manipulate objects in their environment into useful tools. This has enabled them to dominate other species and prosper even in harsh conditions. Eventually *Homo sapiens* conquered the entire planet, and beyond. Overall, all the achievements of mankind can be traced back and attributed, in some way, to developments of the human brain cortex.[2] Considering this, the immense complexity of the brain should not come as a surprise.

For a long time the complexity of the brain has obscured its vital importance to who we are and how we function. In ancient Greece, for instance, scholars believed that the brain was merely a system to cool down our blood, setting us apart from animals by cooling down our primal hot-blooded instincts.[3] In modern times, however, the rather astonishing feats of the brain are properly appreciated, and brain research is hotter than ever. The field of neuroscience has matured as a branch of biology into a multidisciplinary field, studying the nervous system of humans and animals alike. Despite the high effort and progress that have been made, most neuroscientists agree that we have only scratched the surface on brain functionality, and the bulk of the effort remains to be done. Luckily, with the advancements that are being made in other fields such as nanotechnology, neuroscientists are able to study the brain using a host of old and new techniques with continually improved resolution and diversity.

Brain research is both fundamentally and practically of the highest importance. Brain disorders pose an enormous social and economic burden on society. Alzheimer, ALS, Parkinson, epilepsy, and many other brain disorders disrupt lives across all ages, genders, and races.[4] The trend of increased life expectancy of humans has, and will continue to increase the number of people afflicted by some brain related issue. Treating and curing these brain disorders is a strong driver for neuroscience. Furthermore, interfacing with the nervous system to control prosthetic limbs has increased quality of life for many people with reduced physical capabilities by trauma, or since birth.[5]

Others have a more futuristic reason to practice fundamental brain research. In recent years, affluent companies and visionaries such as Mark Zuckerberg, Bryan Johnson, and Elon Musk have in some form expressed interest in, and allocated resources to, brain machine interfacing. These visionaries see an integrated neural interface as an obvious and necessary next step in the evolution of mankind. According to them, merging the mind with machines would significantly increase human capabilities, resulting in a "super-human".[1] The influence of technology in our daily lives has increased exponentially for decades, and some people already have working implants in their bodies such as pacemakers and cochlear implants. According to some, it is also necessary to merge with technology because progress in developing artificial intelligence might render the human race obsolete.[1] The mind-bending implications of these technologies are beyond our capabilities as they are now. As Arthur C Clarke's third law goes: "any sufficiently advanced technology is indistinguishable from magic".[6] Because these technologies are coming closer and closer, debate must be opened now on how we will deal with them socially, economically, and legally, to anticipate the coming difficulties as much as possible.

The medicinal, scientific, and economic value of brain machine interfacing has driven neuroscience forward in the past years. This trend is likely to continue into the future, as technology further enables scientists to expand the collective knowledge of mankind. It is the purpose of this work to reflect on some of the difficulties associated with brain machine interfacing and to explore an approach to counter some of these difficulties. In particular, the conception of a device capable of forming specified connections inside the brain with pre-determined targets is explored. Mainly focusing on specificity as well as the sensitivity and biocompatibility of the device.

Chapter 2: Basic brain morphology

As mentioned in the introduction, the brain is the most complex biological system known to man. In order to provide a contextual framework placing the purpose of this research in the larger scheme, and to justify some technological choices, it is useful to review some basic brain structure and function. The brain consists of two main groups of cells: neurons and glial cells. These cells are surrounded by the extracellular matrix (ECM) that is mostly built up of proteins.[7]

Figure 1 Artistic impression of neural networks in the brain (Artist: Gregg Dunn Title: Self reflected microetching) [8]

Neurons are the cell type most associated with brain tissue. They are the single processing units of the brain. There are approximately 86 billion neurons in an average healthy human brain.[9] Each neuron makes thousands of connections to other neurons, leading to organized networks with a number of interconnections of around a quadrillion, structured throughout the brain. Figure 1 shows an artistic impression of neural networks in the human brain.[8] Furthermore, this vast system is not static, but connections are continuously formed and broken again. The continuously morphing state of the brain is called plasticity. Plasticity is driven by a host of underlying processes and inputs that have not all been elucidated. Despite the complexity of the brain, it is also quite a robust system, sometimes capable of functioning even after extensive physical damage. For example in the case of Phineas Gage, who suffered major trauma after an iron rod was driven completely through his head.[10] However, ageing, trauma and neurodegenerative diseases can disrupt the structure and function of the brain.[11]

Glial cells (oligodendrocytes, astrocytes, and microglia) provide support and perform functions such as maintenance and, to some extent, repair of neural connections and circuits. Oligodendrocytes are myelinating cells. The purpose of myelinating will be explained in more detail later on. Astrocytes (30-65% of the glial cells) provide growth cues to neurons during development, provide mechanical support, buffer neurotransmitters and ions released during chemical signalling, and respond after trauma.[12] Microglia (5-10% of the glial cells) exist in an inactive state until chemical triggering activates them into a more compact state, ready to phagocytose foreign material and produce lytic enzymes. Microglia also produce multiple factors that aid a variety of processes and signalling pathways. Their role in host response to foreign material is not yet entirely understood.[13]

2.1 Neurons

As mentioned earlier, neurons are the primary cell type associated with the brain. Neurons have specialized membranes that can depolarize through ion channels. A membrane depolarization traveling along an axon membrane is called an action potential (AP). Neurons 'communicate' with each other by relaying APs to each other via chemical synapses, which will be explained in more detail later on.[14] Natural conduction of an AP is unidirectional because of the asymmetrical morphology of neurons and the existence of the refractory period, which will be explained in more detail later.[14] Figure 2 shows the structure of two interfacing neurons. The dendrites form the receiving end of the neuron. On the opposite side, the axon forms the transmitting end. The axon hillock is an important site at the base of the axon. When a certain voltage threshold is reached at the axon hillock, the axon is triggered to fire an AP along its length right up to the synaptic terminals, where the AP is converted to a chemical signal in the synaptic cleft. Released neurotransmitter at the synaptic cleft is detected by receptors on the post-synaptic neuron, which then converts the chemical signal back to an AP.[7, 14]

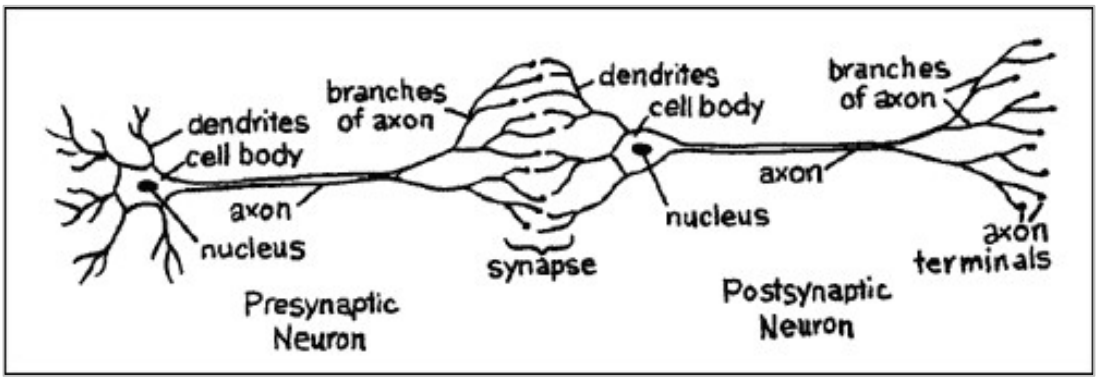

Figure 2 Interfacing neurons (Figure reproduced from [10])

2.2 Action potentials

An AP is a depolarization of the resting membrane potential established by ion pumps and channels in the membrane.[14] An example of the Voltage progression during an AP is shown in Figure 3. A typical resting potential is about -60mV. An AP is a depolarization of the membrane potential up to +50mV. Repolarization caused by potassium ion (K^+) efflux quickly restores the resting membrane potential.[7] The overshoot after repolarization causes a period in which the axon is not able to conduct a signal. This short period in time is called the refractory period. It eliminates the possibility of an action potential returning upstream.[14]

Typically, in the brain axons are partly covered by a myelin sheath. Along the axon there are recurrent unmyelinated zones known as the nodes of Ranvier. In these zones many voltage dependent channels are present, as opposed to the channel deficient myelinated zones. When an action potential travels down the axon, it propagates by means of passive diffusion through the myelinated zones, and is 'refreshed' in every node of Ranvier. This process is called saltatory conduction, and it allows action potentials to travel much faster as compared to unmyelinated neurons.[7]

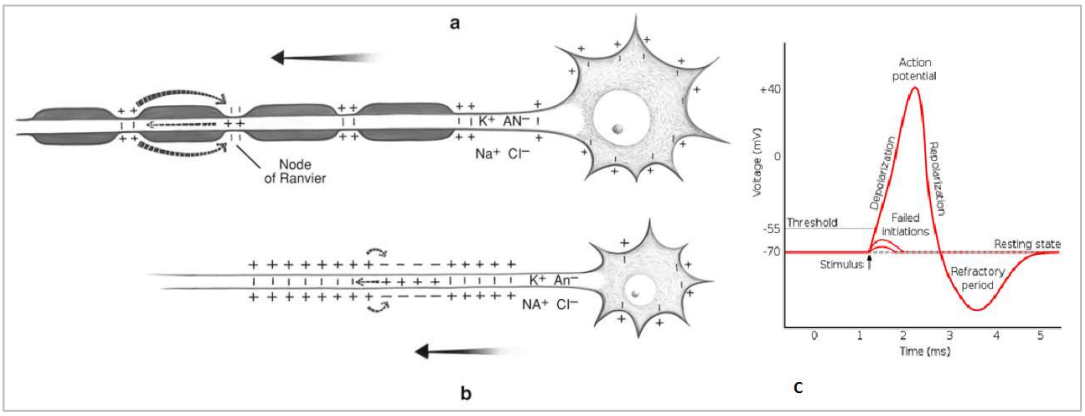

Figure 3 A) Action potential (AP) propagation in myelinated axon B) AP propagation in naked axon C) Voltage progression in a point along a firing axon (Figures a and b and Figure C reproduced from [10, 14] respectively)

2.3 The chemical synapse

Communication between neurons is achieved through electrical and chemical signals at interfaces called synapses. Chemical synapses are asymmetrical structures composed of precisely juxtaposed pre- and post-synaptic compartments. The sequence and timing of synaptic transmission is shown in Figure 4. As an action potential reaches the axon terminus of the pre-synaptic cell, voltage dependent calcium channels are opened. The resulting influx of calcium ions (Ca^{2+}) into the intracellular fluid triggers fusion of neurotransmitter containing vesicles with the cell membrane. The neurotransmitter is then released into the synaptic cleft (the gap between the presynaptic axon and the postsynaptic dendrite). Receptors on the postsynaptic cell, which can be another neuron or alternatively a muscle cell or an endocrine cell, detect neurotransmitter in the synaptic cleft. If the combinatorial signal received from different classes of neurons and synapses is strong enough at the axon hillock of a post-synaptic neuron, an action potential fires along the axon, further transmitting the signal.[7]

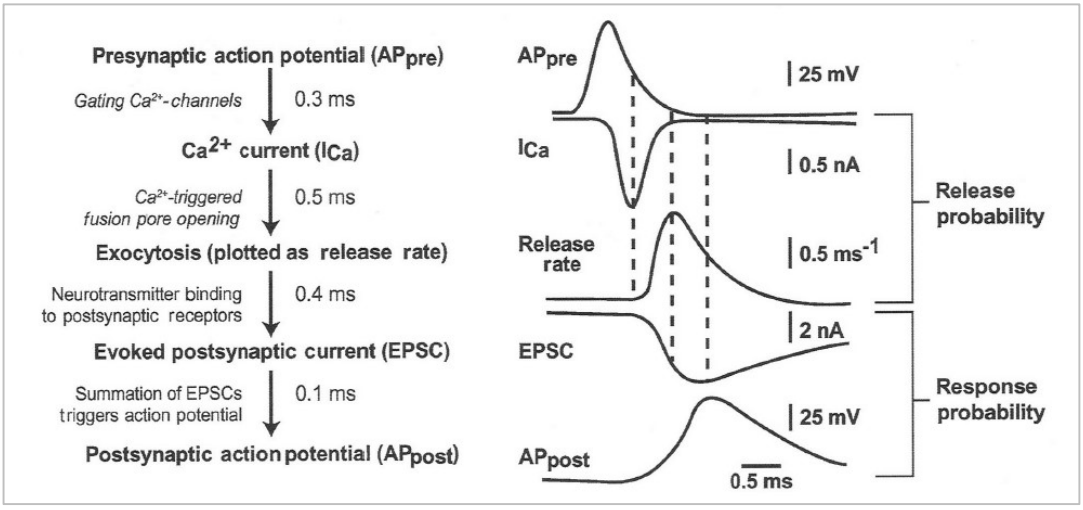

Figure 4 Sequence and timing of synaptic transmission (Figure reproduced from [2])

The contact area of a synapse is 0.2 - 3.1 µm². Within this area there are active zones of 0.05 - 0.10 µm². Active zones are disk like structures with a hexagonal grid. Vesicles containing neurotransmitter are embedded in the depressions of the grid. There are ATP activated protein pumps in the vesicle walls that establish a proton gradient that drives transport and uptake of neurotransmitter. Vesicles have a diameter of about 40 nm, with a protein/phospholipid ratio of about 1/3. Each active zone is associated with >200 vesicles.[15, 16]

2.3.1 Synaptogenesis and specificity

The neuroanatomy of the brain is related to network behavior. Thus, it is clear that when and where synapses are formed, i.e., synaptogenesis, has an effect on how the brain functions. Therefore, spatiotemporal control of synapse formation is of paramount importance for normal brain operation. Synaptogenesis is meticulously controlled through cell signaling, on different structural levels (see Figure 5).[17] The brain is a dynamic structure, which translates to locally continuously morphing structures. In fact, even long established synapses are dynamic structures.[14, 17]

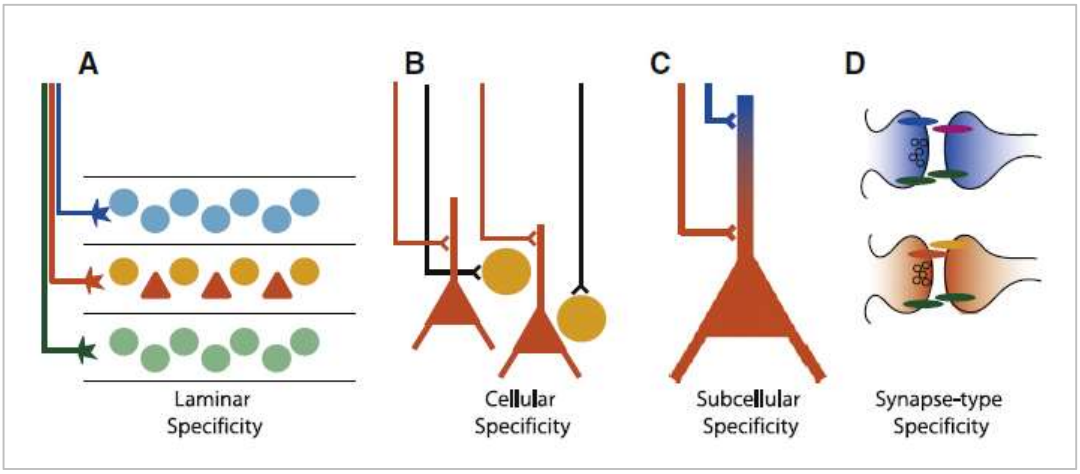

Figure 5 Synapse specificity (Figure reproduced from [17])

Before a chemical synapse can be formed, the pre-synaptic axon must find its way toward the target cell. The direction in which an axon grows is determined by the axon growth cone, which is a specialized sensory motor structure located at the growing end of the neurite. This cone can perceive attracting and repulsing signals, originating either from direct contact signaling or remote chemical signaling. [18] Once the target cell has been reached, a synapse may develop depending on specific signaling. This specific signaling determines the structure and functionality of the synapse by molecularly defined mechanisms. [17] Despite the complexity of synaptic structures, formation can occur within minutes to a few hours. [19]

2.3.2 Synaptogenic proteins

The dynamic and highly organized nature of the CNS calls for tight regulation of synapse formation by neurons. This is, in part, achieved through synaptogenic proteins, which regulate the formation of connections between pre- and postsynaptic cells through contact signaling. One of the best characterized trans-synaptic complexes is the neuroligin-neurexin complex.[20] There are multiple families of synaptogenic proteins that can work either together or independently.[21] Figure 6a and 6b show the modeled protein structure of neuroligin1 (NLGN1) and Leucine rich repeating transmembrane protein 2 (LRRTM2) based

on their amino acid sequence using HADDOCK software. Figure 6c shows a schematic of how these proteins form an extracellular trans synaptic structure between neurons.

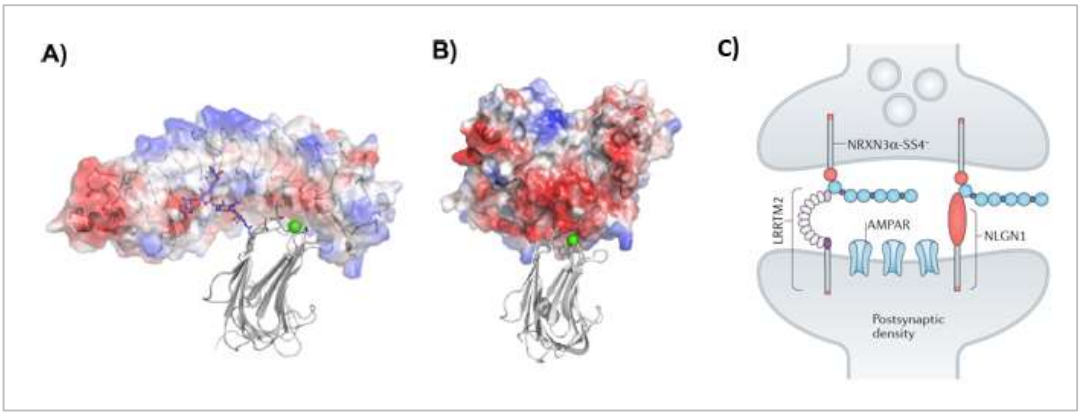

Figure 6 Modelled (HADDOCK) structure for binding structure of neurexin-1β with LRRTM-2 (A) and with NLGN-1 (B) Figures A and B reproduced from [22] Figure C reproduced from [23]

The Neurexin and neuroligin protein families are found in almost all neurons. First identified in 1992, interest in neurexin-neuroligin interaction peaked with a study in 2000 by Scheiffele et al.[24] The study showed that expression of neuroligins on non-neuronal cells is enough to trigger pre-synapse-like structural organization with the functional molecular machinery that releases neurotransmitter vesicles. In order to do this, neuroligin requires a pre-synaptic partner from the neurexin family.[24] Neurexins are a family of proteins that act as receptors on the cell surface.[23] The neuroligin/neurexin trans synaptic complex is about 16 nm long.[18] The function and specificity of synaptogenic proteins originates from diverse functional isoforms of both neurexin and neuroligin due to multiple genes and alternative splicing.[25] There are five neuroligin genes in humans: NLGN1, neuroligin-2, neuroligin-3, neuroligin-4 and neuroligin-4Y.[25] The major extracellular domain of neuroligins is homologous to acetylcholinesterase (AChE), which contains an alternative splice site (A).[26] In NLGN1 1 an additional splice site B is present in the AChE-homologous region. +B NLGN1 1 is localized preferentially at excitatory glutamatergic synapses and binds to neurexin receptors, especially neurexin-1α and neurexin-1β.[25]

Leucine rich repeat transmembrane protein (LRRTM) is a family of synaptogenic proteins that also bind to neurexins, inducing excitatory synapse formation. Four genes code for LRRTM variants: LRRTM-1, LRRTM-2, LRRTM-3, and LRRTM-4, where LRRTM-2 is found to be most effective in synaptogenesis.[27] LRRTM-2 binds to both neurexin-1α and neurexin-1β. Overexpression of LRRTM-2 in cultured hippocampal neurons increases the density of excitatory glutamatergic synapses. Conversely, cultured hippocampal LRRTM-2 deficient neuronal mutants decreases excitatory glutamatergic synapse density.[22, 27]

2.4 Summary

The brain is a complex, dynamic, and highly regulated network of interacting neurons. Information is carried by neurons in the form of action potentials and transmitted between neurons through synapses. The chemical synapse is the main mode of communication between neurons, where neurotransmitter and ion fluxes are used in chemical signaling. Regulation of synapse formation is performed by numerous mechanisms in a range of different structural scales. NLGN1-1 and LRRTM-2 are synaptogenic proteins that are important regulating proteins determining where chemical synapses are formed.

Chapter 3: Recording electrodes

The previous chapter describes the communication between neurons by means of AP's. AP's are membrane depolarizations that can travel along the membrane of a neuron and are transmitted between neurons via chemical synapses. Brain activity can be monitored by measuring these APs. The ion displacement brought on by APs generates extracellular field potentials that can be picked up by electrodes.[28] The recording technique to measure brain activity is evaluated by scale (population of neurons that can be sampled), spatiotemporal resolution and degree of invasiveness. Overall, non-invasive techniques cover a larger volume of the brain but achieve lower spatiotemporal resolution compared to invasive recording techniques. However, contrary to non-invasive recording, invasive recording requires the skull to be penetrated, bringing with it a larger risk for the patient. There are many available techniques to measure brain activity with different benefits and shortcomings. However, given the focus of this thesis, only penetrating intracortical electrodes will be considered. Popular design models for penetrating electrodes are microwires, Utah style arrays and Michigan style arrays (Figure 7).

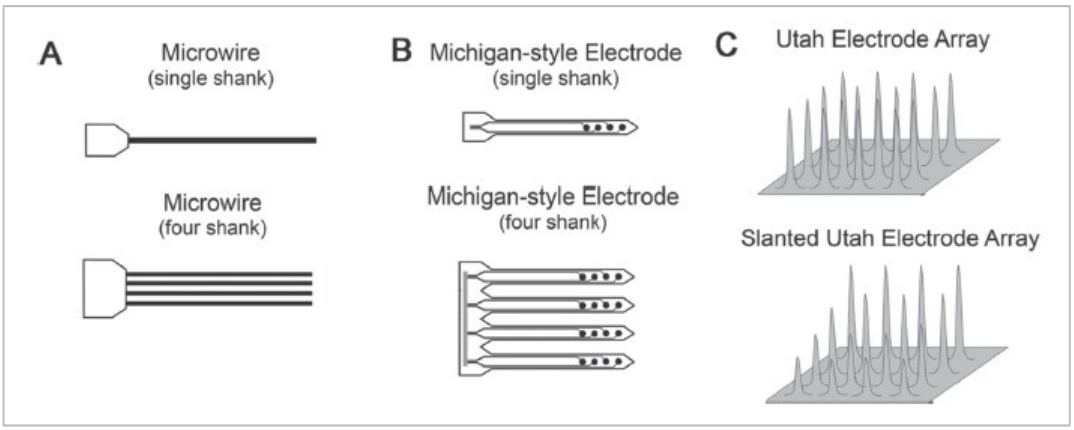

Figure 7 Different electrode styles (Figure reproduced from [4])

The spatial resolution of the probe determines its ability to measure signals from single neurons. A small geometric area of the electrodes is desirable for high spatial resolution. However, a small geometric area increases the impedance of the electrode, decreasing device sensitivity.[29] In recent years, the trend in neurorecording devices has been to increase the number of electrodes with smaller geometric area, up to and over a hundred electrodes per device.[30] This, however, leads to devices with higher impedance, resulting in a need to develop electrodes constructed out of materials with lower intrinsic impedance.[29] Usually, materials used to manufacture electrodes are metals or conducting ceramics. Using materials with a high surface roughness to manufacture electrodes increases the effective surface area up to several orders of magnitude and yields electrodes with lower impedance.[31]

3.1 Microelectrode arrays

The single shank Michigan multi-electrode array (MEA) has a number of electrodes distributed over the length of the probe. The electrodes can measure the ionic current related to action potential propagation from neuron cell bodies. The phase boundary between the electrode and the electrolyte can be modelled by a capacitor. The conducting plates of this capacitor are then considered to be the electrode surface on one side and the electrolyte on the other. The dielectric between the plates exists in the form of a water double layer, consisting of the water dipoles adsorbed onto the electrode and the water dipoles forming the hydration envelope of the electrolyte ions near the electrode surface. This interpretation is called the Helmholtz double layer capacitor.[31] Charge injection into the electrode may occur either through charging and discharging the Helmholtz capacitor at low charge magnitudes (non-faradaic) or through electron transfer across the surface by redox reactions at the surface (faradaic). Redox reactions, however, are preferably avoided. They contribute to electrode fouling by changing the surface properties. Oxidation leads to gas formation, and reduction leads to accumulation of electrons on the electrode surface. Redox reactions may even occur at a zero electrode potential (e.g., rusting of iron).[29, 31]

In neurorecording, the distance between the electrode and the neuron influences the strength and quality of the recorded signals. The maximum recording range of electrodes has been estimated to be roughly 50-150 µm.[32] Thus, the maximum recording distance is about ten times the cell body diameter. This narrow range, combined with inter-subject variability, makes it impossible to reproducibly target single neurons. The amplitude of action potentials in the CNS can be over 500µV, but they are usually only 100µV or smaller.[33] Because of these low potentials, often Local field potentials (LFPs) of groups of neurons are measured instead of single unit recordings.[34] Undistinguishable action potentials originating from surrounding neurons cause background signals called neural noise. Usually, a signal to noise ratio of at least 5:1 is required for accurate measurements.[33] Electrode impedance, combined with the capacitance between the electrode and the amplifier, also affects the electrode's ability to record high frequency signals.[33] Recording electrodes are usually characterized by their impedance at the biologically relevant frequency of 1kHz. In vivo impedance values at 1kHz of 50 kOhm to 1000 kOhm have been reported. [33]

For this research, electrode arrays were provided by the Life science technology and imaging (LSI) group at Imec. They consisted of chips with 14 pairs of Titanium nitride (TiN) electrodes (Figure 8). The sizes and configuration of the electrodes on the chip can be found in appendix A.

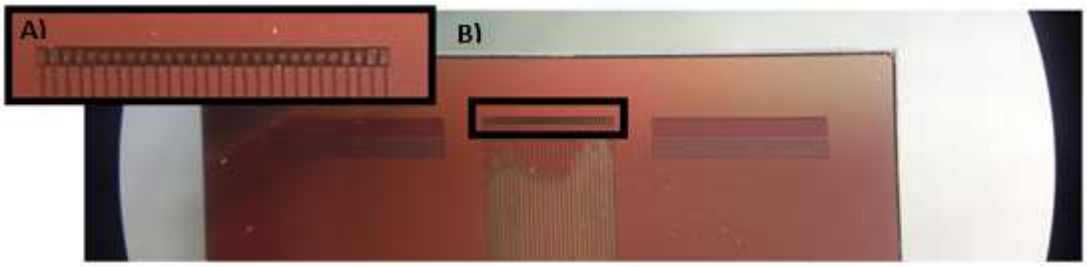

Figure 8 A) 28 electrodes close up B) Chip close up

3.2 Titanium nitride

Titanium nitride (TiN) is a polarizable conducting ceramic. Due to its biocompatible properties, TiN is considered to be a good coating material for cortical electrodes. Sputter deposition of TiN produces a porous layer with a high surface area (Figure 9b). Small electrodes can be fabricated with limited impedance increase due to the highly porous surface geometry of the TiN layer. Water reduction and oxidation potentials (water window) of -0,9V and 0,9V, respectively, have been measured by slow-sweep-rate cyclic voltammetry. This range is wider than that for platinum electrodes or iridium oxide electrodes. Within the water window range, reaction with water (hydrolysis) does not occur, preventing breakdown of the electrode material, thus maintaining electrode integrity.[31] Metals used in electrode fabrication interact with oxidants in the environment to convert to a more chemically stable form (corrosion). TiN also corrodes at zero electrode potential in water. However, the reaction is very slow and does not lead to significant damage.[31]

Because of its chemical and mechanical stability, the TiN coating is not sensitive to dehydration, can be sterilized by common methods, and can easily be transported or stored, wet or dry. TiN is also suitable for deposition on flexible substrates. Cathodic voltages are more harmful to TiN than anodic voltages. Figure 9a shows a cyclic voltammogram of a TiN electrode. The inflection points on the graph (red arrows) indicate where current increases as a consequence of hydrolysis of water and gas evolution. [31, 33]

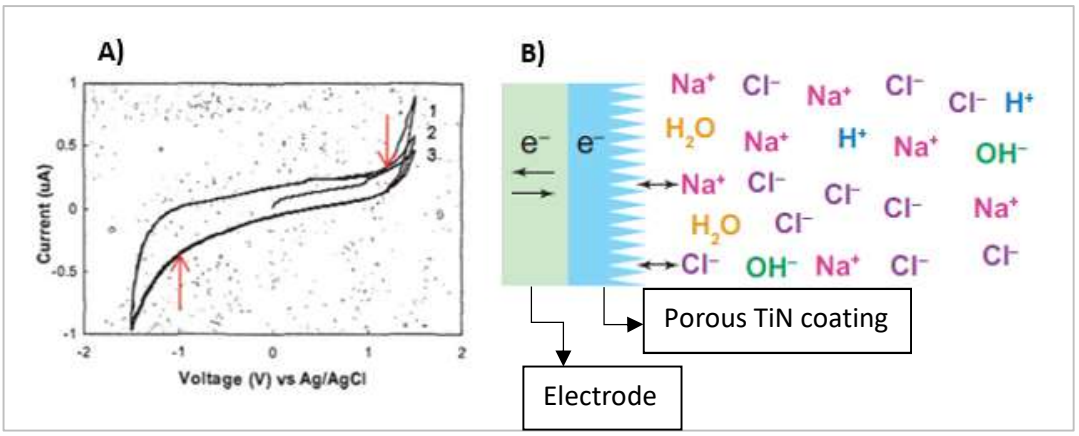

Figure 9 A) Cyclic voltammogram of TiN (left arrow reduction, right arrow oxidation) (Figure reproduced from [31]) B) Schematic of a TiN coating (Figure reproduced from [33])

The White Matter LLC NanoZ™ device was used for measuring the impedance of the electrodes. The chips were glued and wire bonded to printed circuit boards (PCBs) of our own design (see appendix B). The wire bonds were protected with a glob top cover. Pin adaptors were soldered to the PCBs to make them compatible with the NanoZ™ adaptor NZA DIP16. The electrodes were mapped in the NanoZ™ software (see appendix C). Using the setup shown in figure 10 the initial impedance of the electrodes was measured in phosphate buffered saline (PBS) with a platinum wire counter electrode.

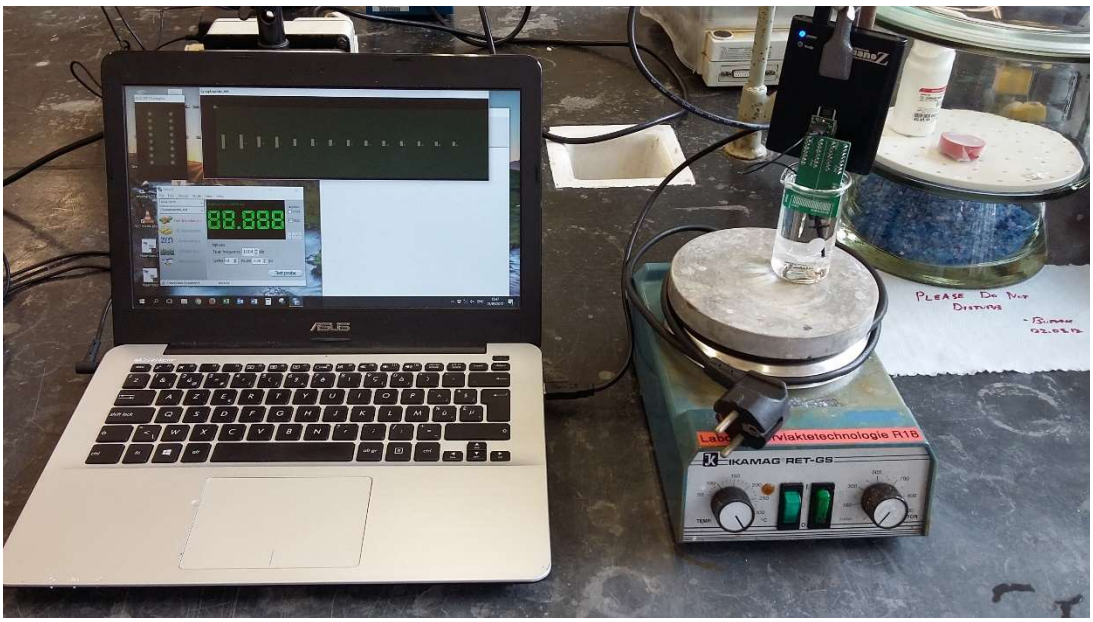

Figure 10 NanoZ Impedance measurement setup

Figure 11 shows the measured impedance values of the untreated chips. Initially, the impedances were higher than expected. After some cleaning steps (sonication, water rinse and isopropyl alcohol (IPA) rinse), the measured impedances became increasingly small until a stable point (< 0,05 MOhm) was reached where the impedances no longer changed. These values were found to coincide with the results obtained by the LSI group (results were confidential, but were confirmed). All measurements were performed in triplicate and averaged (for calculations see appendix D).

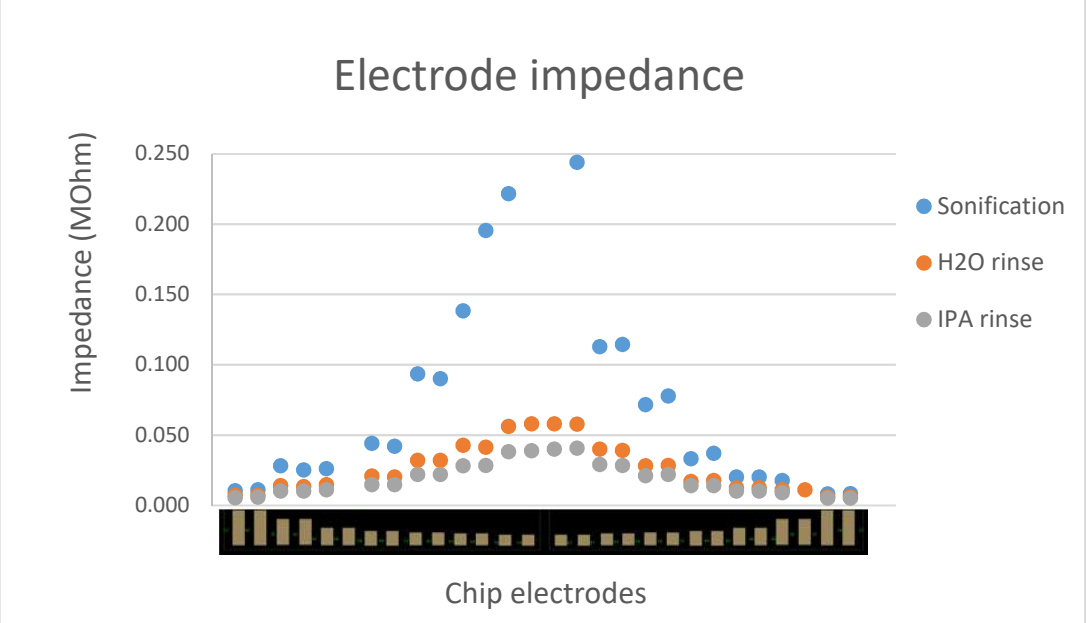

Figure 11 Initial electrode impedance values

3.3 Biocompatibility

Implanting MEAs into the brain elicits a response of the biological tissue to the foreign object. The extent of the host response is a measure for the biocompatibility of the probe. Every implanted probe will elicit a response to some degree, but comparatively the response elicited by more biocompatible materials will be less. A schematic diagram of probe insertion and subsequent host response is shown in Figure 12. Figure 12a shows a inserted probe with surrounding brain tissue immediately after insertion. The tissue has not had the time yet to respond to the foreign material, undamaged cells in surrounding tissue remain unaltered. Figure 12b and c show a diagram of the acute and chronic host response, which will be discussed in more detail later on.

The host response causes the quality of the signal picked up by the electrodes to diminish over time. Long-term recording over a clinically relevant period of time is difficult because of this loss in signal quality. It is therefore imperative to mediate the host response as much as possible.[35] There are several techniques to approach this problem in device design, which will be addressed later. First, an overview is given of the timeline and mechanisms of the foreign body response of the brain to probe insertion. In literature, the evaluation of the host response to probe insertion is mostly based on a binary system of being either acceptable or unacceptable. Further description is often omitted. The timescales are usually divided into the acute response and the chronic response. [29, 36]

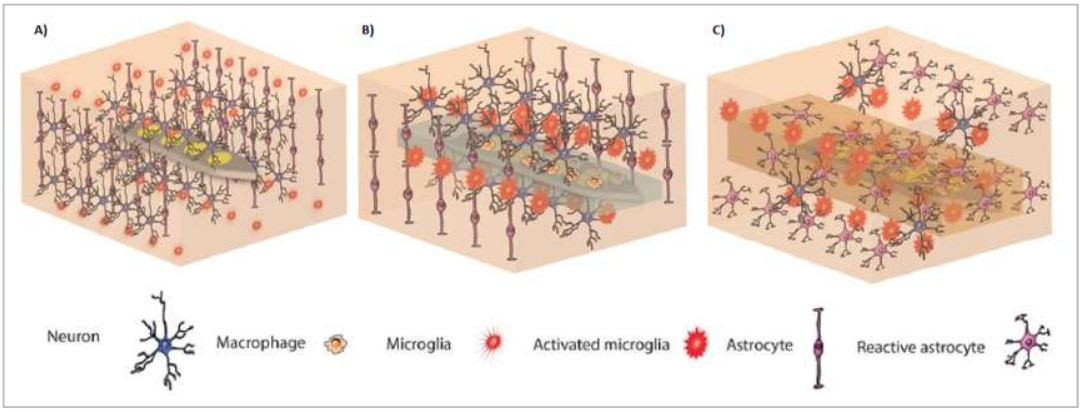

Figure 12 Schematic of foreign body response after probe insertion (Figure reproduced from[29])

In order to measure LFPs in the cortex, probes must first be inserted into the brain. Few studies examine the impact of the initial penetration, but the effect is considerable. The needle like probe rips through ECM, capillaries, and glial and neuronal cell processes. This initiates a wound healing process similar to that in other tissues. Disruption of blood vessels releases erythrocytes and activates platelets, clotting factors, and the complement cascade to aid in macrophage recruitment, causing swelling of the tissue surrounding the inserted electrode and possibly pushing target neurons further away.[29, 35]

As quickly as one day post implantation, this acute inflammation reaction recruits and activates microglia. [37] These activated microglia secrete cytokines and chemokines, further recruiting macrophages and activated microglia, and further promoting the host response. Cytotoxic and neurotoxic factors, such as excitatory amino acids and reactive oxygen intermediates, are also produced, leading to neuronal death. Astrocytes are activated into the reactive phenotype after trauma, enhancing migration, proliferation, hypertrophy, expression of glial fibrillary acid protein (GFAP), and matrix production. Identifying astrocytes and the degree of activation within a population is conventionally done by GFAP staining.[37, 38]

After 6-8 days, the activated microglia have removed most cellular debris and damaged matrix through phagocytosis.[29, 38] Because the probe is too large to be cleared by the activated microglia and astrocytes, the host response persists. In this stage of chronic inflammation the microglia merge together in an ultimate attempt to phagocytose the foreign material. Glial scar is formed by both reactive astrocytes and activated microglia. Colonies of microglia remain at the surface of the implanted electrode. These microglia produce a thin layer of ECM proteins, mechanically strengthening the encapsulation structure surrounding the foreign material, called the basal lamina. Lytic enzymes and reactive oxygen agents are also released in an attempt to degrade and remove the foreign object. The glial scar tissue acts as an insulator between the electrode and the target neuron, further increasing the impedance of the tissue-electrode interface, enhancing noise levels and decreasing target signal strength. [29]

A lot of attention has been given to the behavior of non-neuronal cells in the host response, but much fewer research has been done on the impact of the host response on neuronal cell population. Reduced neuronal cell population is observed around the site of implantation.[39] As mentioned before, activated glial cells produce cytokines and chemokines that cause neural cell death. Also, it has been suggested that failure to phagocytose foreign material leads to a state of frustrated phagocytoses, a state where neurotoxins are continuously released, further contributing to neural cell death. Hence, neural density often decreases in the vicinity of the implant. Kill zones between 1 and more than 100 micrometers around the implant have been reported.[37]

Figure 13 shows the neuronal cell body population around a stab wound site (figure 13a and c) or an implant site (Figure 13b and d) at 2 weeks (Figure 13a and b) and 4 weeks (Figure 13c and d) after operation. The neural population of brain tissue after a stab wound is undifferentiable from healthy tissue as indicated in Figure 13e and f. However, in the immediate vicinity (0-100µm) of an implant neuronal population is significantly reduced as compared to control samples (ANOVA, $p<0,05$).[37]

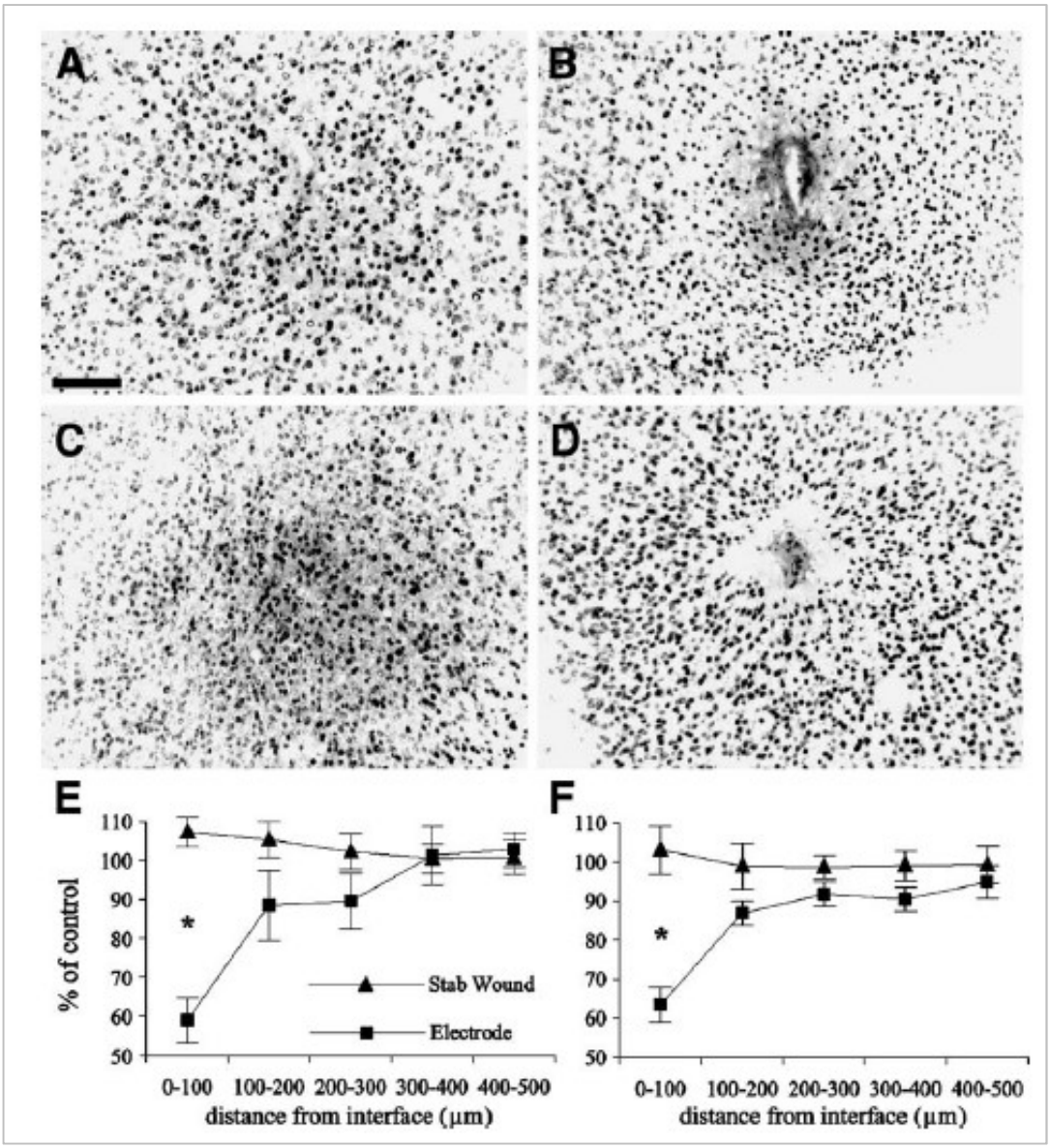

Figure 13 Neuronal cell population around implantation site (scale bar 100µm) (Figure reproduced from [37])

3.4 Summary

MEAs are inserted into the brain cortex to measure local field potentials, in order to derive brain activity in subjects. Spatio-temporal resolution of the measurements depends on probe design and placement, but is also dependent on the host response, which causes signal quality to diminish over time. Materials like TiN are used for electrode design because of their good biocompatibility and reduced impedance compared to other materials such as gold. Impedances were measured of Chips with TiN electrodes provided by the LSI group at Imec with a White Matter LLC NanoZ^{TM} and found to coincide with the original measurements done by the LST group.

Chapter 4: Surface modification

The previous chapter describes the host response of the body to the insertion of a probe. Attempts to mediate host response range from changing tip shape, to using bioactive molecules, to incorporating live cells into the design (hybrid devices). Biological tissue prefers a hydrated environment, is soft and dynamic, and functions with ionic charge carriers whereas metals prefer dry environments, are hard and static, and function with electrons as charge carriers. These inconsistencies between biological tissue and the electrode material can worsen the host response.[38] The electrode surfaces of neural probes can be modified with appropriate materials in order to increase device performance or to limit the aforementioned inconsistencies. Nanostructured materials can provide an excellent foundation for nanoelectronics design. [29, 40, 41]

4.1 Conductive polymers

The conductivity of conductive polymers (CPs) originates in their chemical composition. As illustrated in Figure 14, the backbone of CPs is a conjugated system formed by a series of alternating single (σ) and double (π) bonds. The electrons of the single σ-bonds provide strength to the backbone chain, whereas the electrons of the double π-bonds are delocalized. This generates a valence band and a conduction band with a bandgap of 1,6-1,7eV, resulting in a system that acts as a semiconductor. [41, 42]

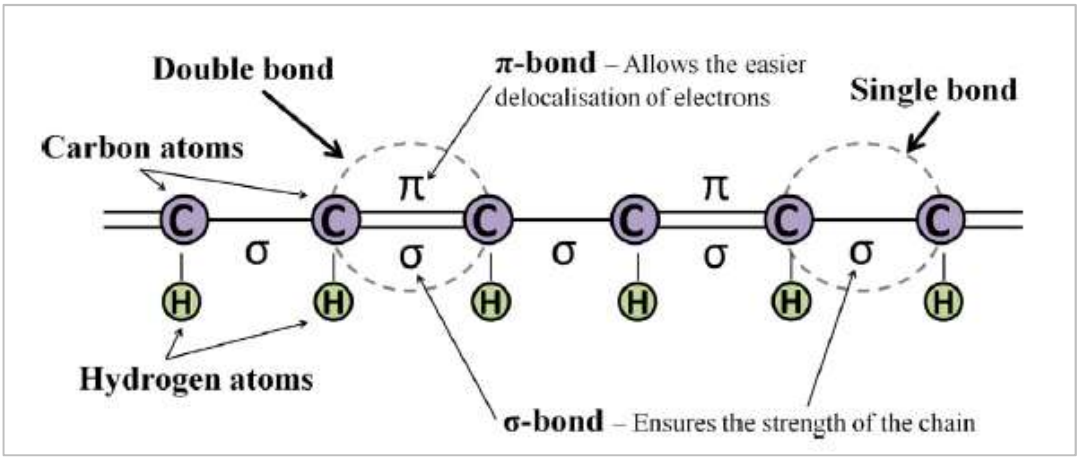

Figure 14 CP backbone chemical structure (Figure reproduced from [41])

To become a good conductor this semiconductor system needs positively or negatively charged dopants. The dopant adds a positive or negative charge to the system. A localized charge, called a polaron, is created on the conjugated backbone (Figure 15). It is energetically favorable for this polaron to be localized somewhere on the chain, instead of being delocalized. When a potential is applied, the loosely held polaron can move from one

side to the other, giving the polymer its conductive property. For the high electronic conductivity that is required for low-impedance recording or for charge-injection, anionic doping is necessary. Anionic doping results in a negatively charged polaron (an electron) with higher mobility as compared to positively charged polarons (holes). Charging and discharging of the polymer is achieved through a reversible redox reaction. This is accompanied by the movement of ions and solvent into or out of the polymer, causing a volume change of the CP layer. Electrical, mechanical and chemical properties of CPs are closely related. Electrochemical oxidation and reduction can alter properties like wettability, color, volume, and conductivity. The choice of dopant will affect the conductivity and also the surface morphology of the CP network. Commonly used anionic dopants are para-toluene sulfonate (pTS, Figure 15b) and polystyrene sulfonate (PSS, Figure 15c).[41]

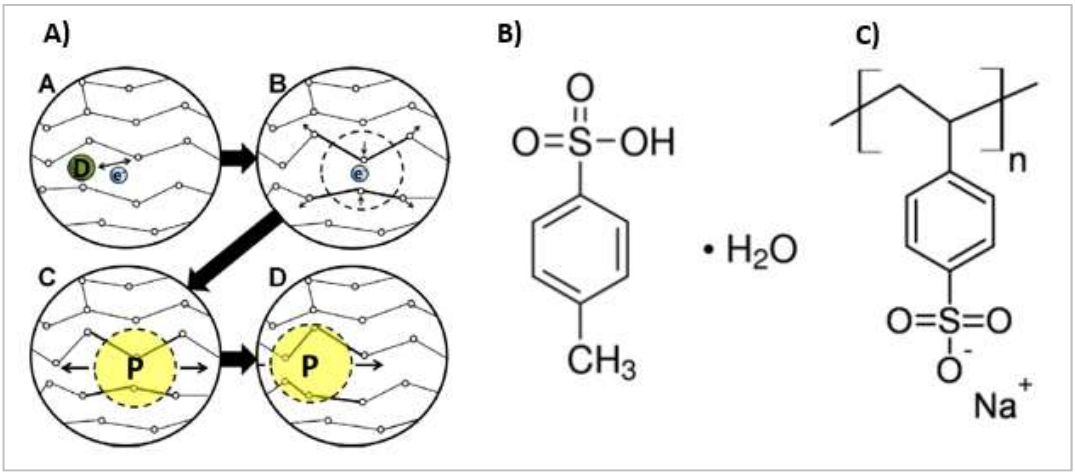

Figure 15 A) Polaron localization on the CP backbone (Figure reproduced from [41]) B) pTS C) PSS

Since the discovery of polyacetylene in the 1970s interest has grown in the use of CPs. CPs have been regarded as promising materials for surface modification due to their ability to transfer the electrical charge from ions in living tissue to electrons in an electrode, combined with their chemical diversity, lowered Young's modulus compared to metals, and tailorable topological properties.[41] The biocompatibility and tissue interactions of CPs can be altered by incorporating biomolecules and/or therapeutic agents into the polymer network.[29, 40] The incorporated biomolecules have a significant impact on the mechanical and adhesive properties of the polymer layer, depending on their size, charge, and manner of incorporation.[29, 41, 43]

Multiple CPs are now known and used in a variety of biomedical applications, including neural interfaces. CP coated electrodes have been shown to exhibit superior charge transfer capacity and reduced impedance.[29, 40] Among the most used are poly(pyrrole) (PPy), poly(aniline) (PANI), and poly(3,4-ethylenedioxythiophene) (PEDOT) and derivatives.[41] PPy is arguably the most researched CP. However, because of superior conductivity and long term stability, PEDOT has gained much interest in recent years. The PEDOT polymer is built up of repeating units of EDOT monomer (Figure 16). Due to the dioxyalkylene bridging group

on the thiophene ring, the bandgap is lowered along with oxidation and reduction potentials. This gives PEDOT improved conductivity and stability. [29]

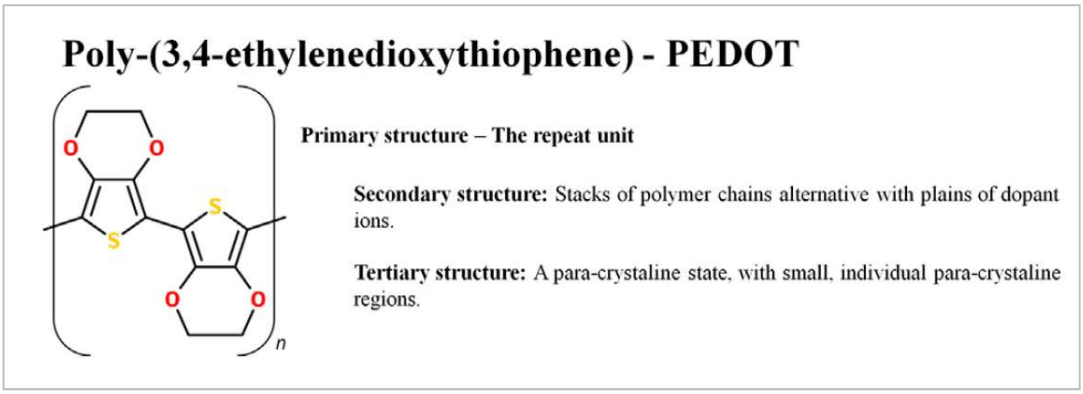

Figure 16 PEDOT primary structure (Figure reproduced from [41])

Two main methods are used to synthesize PEDOT: chemical and electrochemical synthesis.[44] The advantage of electrochemical synthesis is that the polymer only forms on conductive surfaces. This situation is ideal for electrode surface functionalization. Electrodes are placed into a solution containing EDOT monomers, solvent, and doping agent. Electro-polymerization is usually performed in organic solvents because the thiophene structures are poorly soluble in water but also because organic solvents have an oxidation potential higher than that of water. Also the formation of thienyl cation radicals is catalyzed by water, and thienyl cation radicals activate other reactions that hinder the formation of the main polymer. Choosing a suitable water-soluble polyelectrolyte like PSS as an emulsifier allows the electrochemical deposition of EDOT in aqueous medium. The positively charged active electrode is the surface upon which the polymer will form. The negatively charged counter electrode remains free of polymer. The monomers are deposited and oxidized on the working electrode, forming the polymer. The dopants are physically entrained in the PEDOT layer during electro-polymerization and form a charge-transfer complex that results in the oxidation of the PEDOT. Coating electrodes with a conductive PEDOT layer significantly reduces impedance by increasing the effective electrode surface and improves biocompatibility.[41]

Electrochemical deposition can be performed by potentiostatic, potentiodynamic, or galvanostatic methods. [41, 42] The potentiostatic method keeps the potential constant, while varying the current. This method protects the integrity of the components and is most suitable for biosensor manufacturing. For example, the morphology of the formed layer varies with the applied voltage used for electro polymerization (Figure 17). At 0,90V the formed layer has a globular morphology. With increasing voltage, the layer becomes more spongiform. These tests were performed on stainless steel that was roughened by sand blasting to increase adherence of the PEDOT layer.[45]

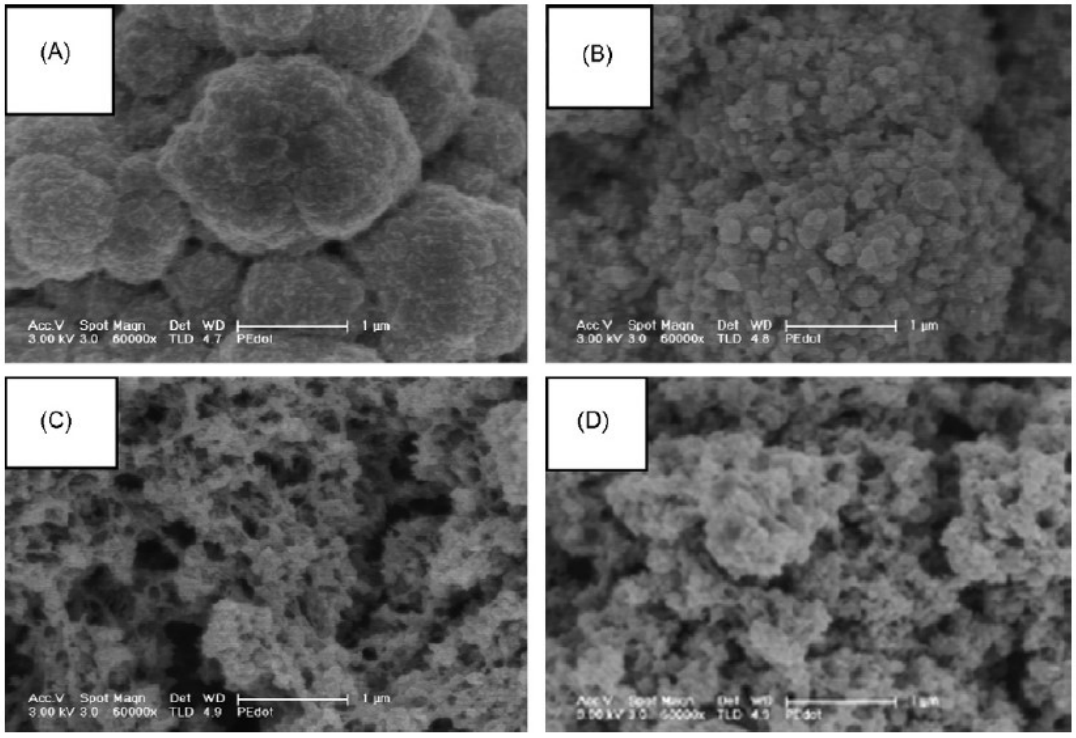

Figure 17 potentiostatic polymerization on stainless steel with different voltages. (A) 0,90V, (B) 1,00V, (C) 1,10V, (D) 1,20V (Figure reproduced from [45])

There are a couple of ways to functionalize a PEDOT layer: adsorption, covalent binding, entrapment, and crosslinking. [41]

- Proteins can be linked to the PEDOT surface by nonspecific adsorption, through Van der Waals forces or ionic charge attraction. Adsorption may affect protein activity or even destroy functionality. It can also be reversible.

- If proteins are mixed with the solution during electrodeposition, they can become physically entrapped in the polymer matrix. This will influence the morphology of the layer and on the activity of the protein because the encapsulation causes the active sites to be less accessible due to steric hindrance.

- Because there are no chemically active groups present on PEDOT, it needs to be chemically modified before covalent grafting becomes possible. This modification will affect the conductivity and morphology.

- Some proteins can be crosslinked with the CP through the same polymerization pathway, provided the needed chemical groups are present. Crosslinking proteins into the polymer network by adding them during electrodeposition will have grave effect on the conductivity, because the conjugated system will be broken, and on morphology.

For this research TiN electrodes were modified with PEDOT/pTS. No literature was found where this was attempted before. Therefore, the procedure was modeled after electrodeposition of PEDOT on platinum electrodes.[46] After some trial and error testing, EDOT/pTS 0,1M/0,05M in H2O/MeOH 1/1 with a 1-2 mA/cm² current flow were found to be good conditions for electrodeposition (reagents see appendix E). Electrodeposition was performed for 15 minutes, resulting in an impedance drop of about 1 order of magnitude. Figure 18 shows the results of two electrodes that were PEDOT coated using the conditions described above. Electrode pair 1 (E1) were 70x70 µm in size and electrode pair 2 (E2) were 60x60µm in size. Each time 1 of the electrode pairs was coated (modified) while the electrode next to it was left untreated (control). SEM pictures of the untreated and treated electrode pair 2 can be seen in Figure 19a and Figure 19b, respectively. The morphology of the formed nodular PEDOT:pTS layer is comparable to that found in literature.[42]

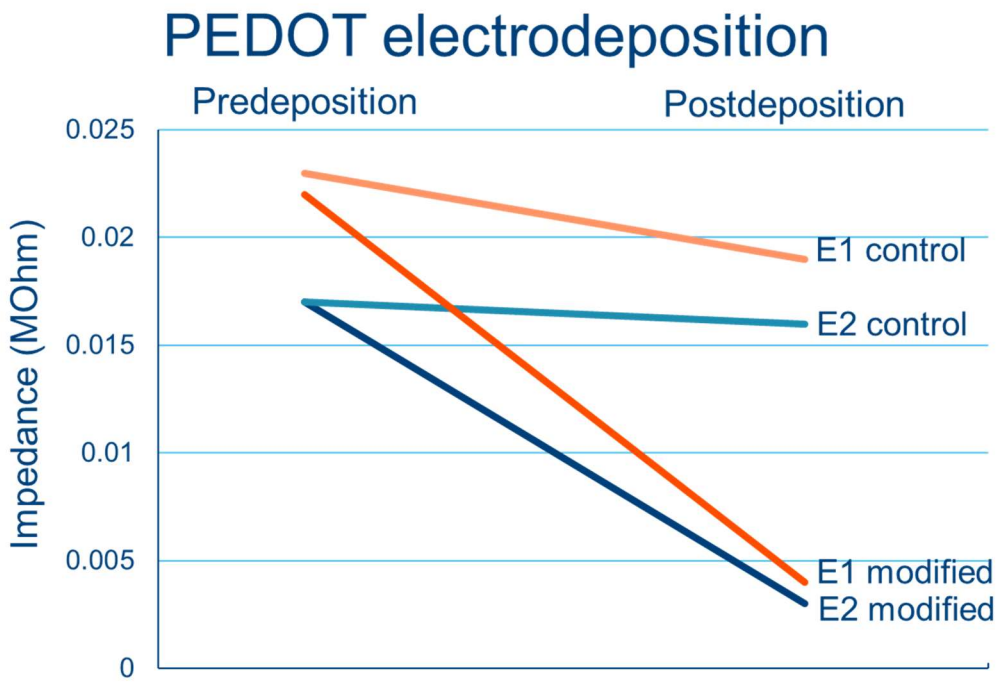

Figure 18 Impedance drop after electrodeposition of PEDOT

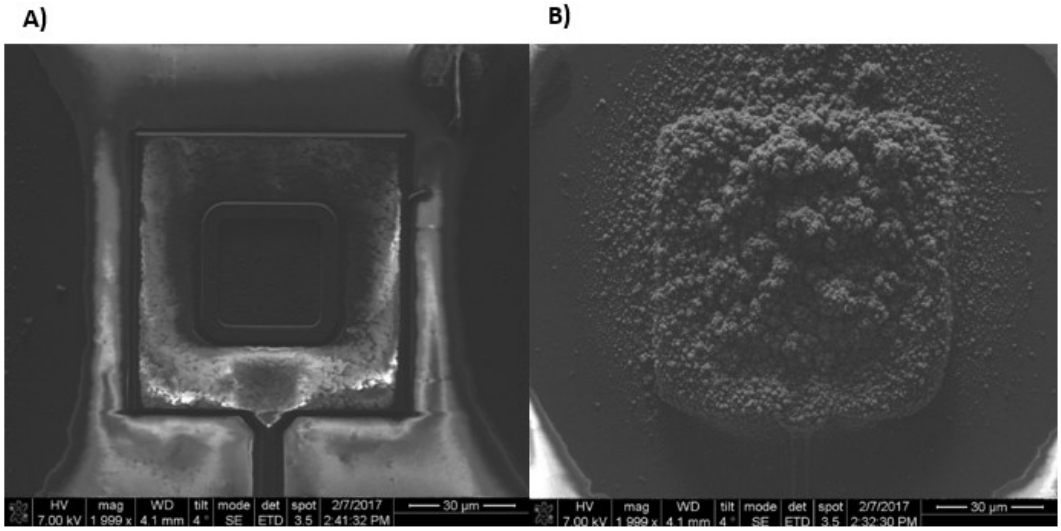

Figure 19 A) Untreated TiN electrode B) Modified TiN electrode

4.2 Hydrogels

Hydrogels (HGs) are networks of crosslinked hydrophilic polymers, capable of absorbing up to 99% by weight of water. As mentioned before, the biological environment in the brain also has a high water content, making HGs an attractive candidate for neural interfacing.[44] Permanent HGs can consist of natural or synthetic polymers, crosslinked by covalent bonds. Classification of HGs can be done by source, structure, charge, appearance, or composition. The HG properties can be tuned by choosing different compositions and degrees of crosslinking.[47]

HGs have been extensively researched as 3D scaffolds for tissue engineering applications and drug delivery. Overall, synthetic HGs have poor cell interaction, making them useful as anti-fouling coatings for electrodes. Incorporation of a natural polymer like collagen can improve cell adherence.[48] The Young's modulus of brain tissue is less than 100 kPa. Some HGs have a Young's modulus that is approximately the same, reducing micromotion damage. However, if the Young's modulus is too low, insertion becomes a problem due to delamination of the HG coating from the electrode surface.[44]

Although HGs are considered poor conductors, due to their open structure, most are also poor insulators. Therefore, deposition of a thin layer of HG onto an electrode should not have a dramatic effect on electrode impedance. It has been observed, however, that due to swelling of the HG in vivo, the target cells are pushed away. The further away the target cells are pushed, the weaker the signal that can be picked up by the electrode.[47]

Polyvinyl alcohol (PVA) is a synthetic polymer consisting of repeating vinyl alcohol monomeric units. It is synthesized in a two-step process of first free radical polymerization of vinyl acetate in an alcoholic solution, followed by partial hydrolysis of the acetate function to a hydroxide function. PVA has some useful properties such as water solubility, some biodegradability, excellent biocompatibility, low toxicity, film orientation characteristics and adhesive properties. Highly hydrolyzed PVA results in macromers with densely packed

hydroxyl groups, highly interacting with hydrogen bonds. This causes lower water solubility and reduced availability of the hydroxyl groups for chemical modification. The residual acetate groups are hydrophobic in nature, and weaken the intra- and intermolecular hydrogen bonds. [48]

For HG synthesis, photopolymerizable sidechains need to be linked covalently to PVA macromers. A protocol derived from Coburn et al. (2012)[49] was used; PVA 27000 Da (Mowiol 4 99%) was purchased from Sigma Aldrich and used without further purification. A 5% PVA solution was prepared at 80°C. A 1/1 ratio of glycidyl methacrylate (GMA) to repeating unit of PVA was added, and the pH was adjusted to 1,5 using HCl. The reaction was allowed to proceed overnight at 60°C. The polymer was precipitated in acetone and redissolved in water. The solution was then dialyzed with a 10kDa cut-off dialysis tubing. The purified sample was lyophilized and stored for further use.

The degree of methacrylation of the samples was analyzed by ^{1}H NMR. The peaks corresponding to the GMA group were compared to the peak originating from the PVA backbone. ^{1}H NMR spectra of unmodified GMA and PVA are shown in figure 20. For GMA, the hydrogen peaks corresponding to 6,1 and 5,8 ppm (peaks d in Figure 20) were used. For PVA, the peak at 4 ppm was used (peak F in Figure 20). The ^{1}H NMR results of the modified PVA macromers is shown in Figure 21. The area of the methacrylate side chains was found to be 0,006% of the PVA backbone. This value was used as the degree of methacrylation (%Methacrylation).

The number of GMA cross linkers per chain were calculated via the formula:

$$Cross\ linker\ per\ chain = \%Methacrylation\ x\ \frac{MWpolymer}{MWrepeating\ unit} = 0{,}006\ x\ \frac{27000}{44} = 4$$

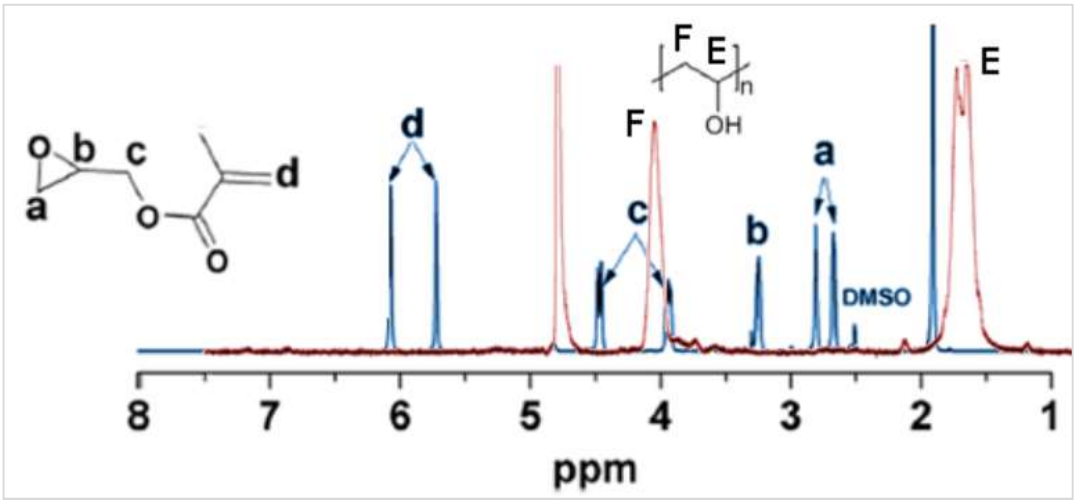

Figure 20 ^{1}H NMR spectra of unmodified GMA and PVA (Overlay of Figures reproduced from [50] [51])

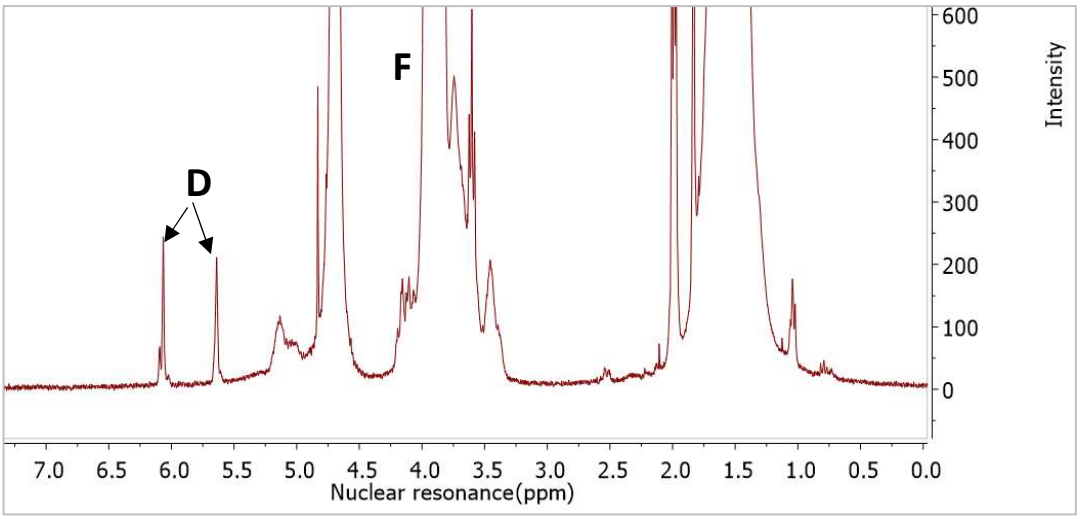

Figure 21 [1]NMR result of modified PVA Areas peaks D: 1000 and 1055; area peak F: 16466890

To photopolymerize the PVA-MA, 0,1% Irgacure 2959 was left to dissolve in water overnight in a 40°C incubation chamber, and vortexed until dissolved. 20% of the lyophilized PVA-MA was added and dissolved at 80°C. The solution was then pipetted into molds and photopolymerized at 365nm for 30 minutes. The resulting HGs were cylindrically shaped with a diameter of about 5mm (see Figure 22).

Figure 22 PVA HG disks

Using the same procedure, the HG precursor solution was prepared, deposited on top of PCB gold pads, and photo-crosslinked. The deposition was performed by hand using a micro pipet, and spread using a pipet tip. Uniformity of the layer is not guaranteed, but is sufficient for the testing phase. The gels were left to dry overnight for optimal adhesion. Next, the gels were rehydrated and impedances were measured (see Figure 23). Because the gold pads on the PCBs were not designed to be used as electrodes there is higher tolerance toward variance in their production. This is reflected in the higher variance in measured impedances. The mean values and standard deviations were calculated (Figure 24) omitting the first and last electrode results, since no HG was deposited there (Figure 23). A standard

Student two-sample t-test was performed to confirm that the means of the two populations were significantly different with a 5% significance level.

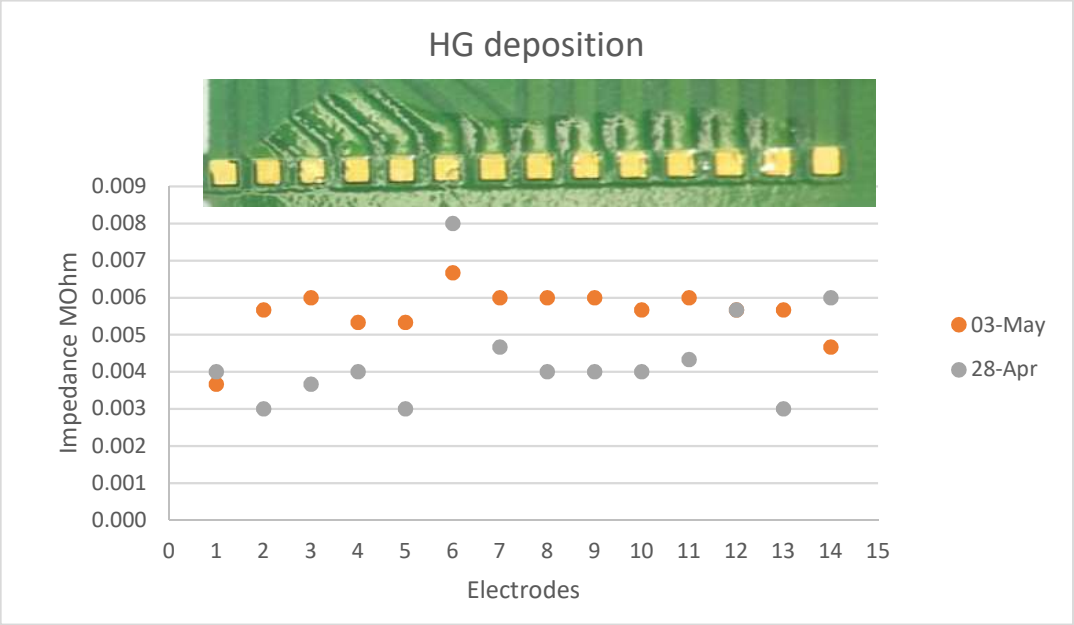

Figure 23 Impedance results before (28-Apr) and after (03-May) deposition

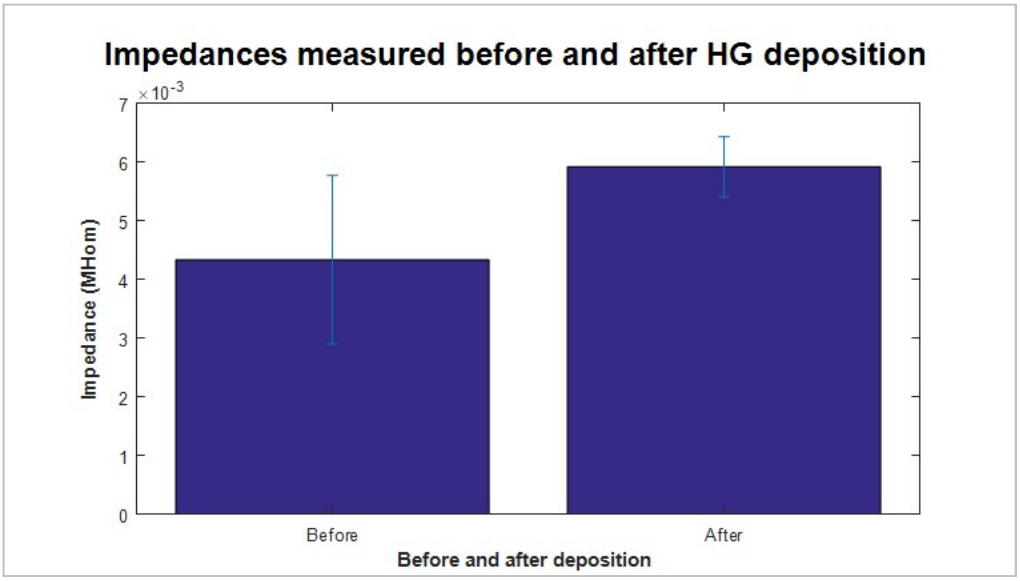

Figure 24 Error bar graph impedance results of electrodes 2-14 before and after HG deposition (averages significantly different with p<0,05)

4.3 Interpenetrated networks

The conductivity of PEDOT polymers and the biocompatibility and functionalization possibilities of PVA suggest that, combined, they could potentially form a very interesting system for brain-computer interfacing. However, synthesizing a truly interpenetrated network of these two dissimilar polymers is not trivial. When a conductive polymer is electrodeposited onto an electrode there are some mechanisms of nucleation that need to be considered (see Figure 25).

Primary spontaneous nucleation occurs at the electrode surface. During polymerization, the monomers are oxidized under a positive charge. The voltage at which this takes place is dependent on the monomer, the dopant and electrolyte during the polymerization process. When a critical chain length is achieved, the oligomers precipitate out of solution. Primary spontaneous nucleation will occur at the electrode interface because the oxidation potential for polymerization is the lowest there. When attempting to form an interpenetrated network (IPN) of HG and CP, the formation of the CP will start at the electrode interface and grow thicker, pushing the HG layer outward. This results in a phase separated electrode surface that has a HG layer on top of a CP layer, resulting in higher impedance, and increased delamination risk. In order to synthesize a true IPN it is necessary to introduce nucleation sites inside the HG, which allow primary and secondary nucleation to occur within the HG. Nucleation sites within the HG can be introduced by covalently binding charged molecules. This locally minimizes the Gibbs free energy, allowing reduction of the monomers. In this way, polymers are formed inside of the HG due to the presence of charged foreign particles, independent of the electrode surface. Secondary nucleation allows growth of the oligomer chains until an IPN is formed.[52]

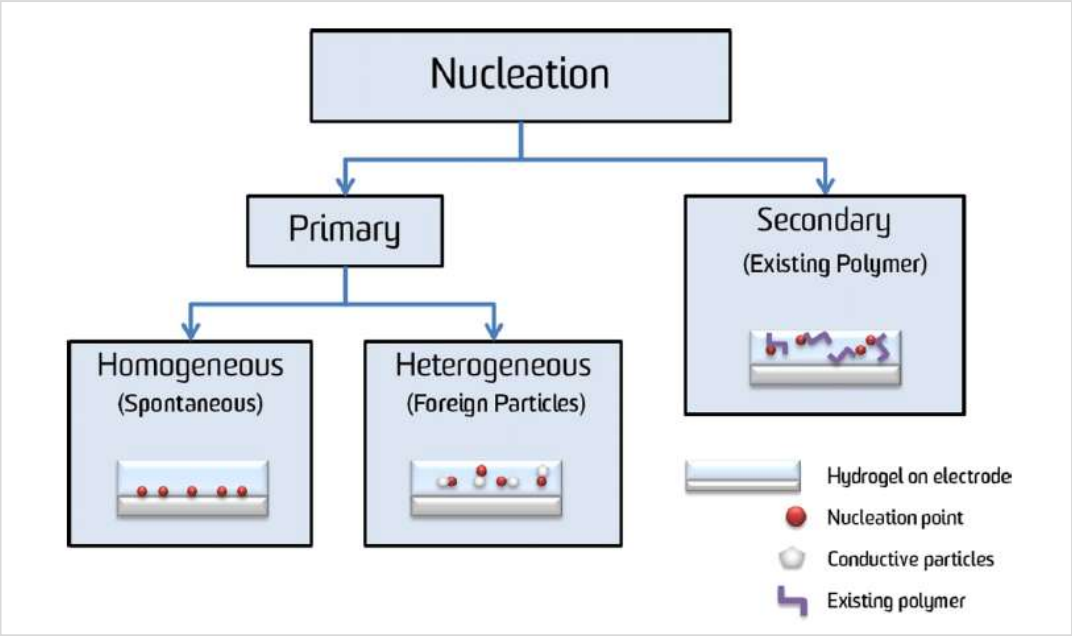

Figure 25 Nucleation mechanisms of CP on HG covered electrodes (Figure reproduced from [52])

Therefore, charged molecules need to be introduced into the HG prior to electrodeposition. Green et al. (2012)[53] were able to synthesize a conductive HG (CHG) by growing PEDOT electrochemically through a PVA-Heparin combined HG. The localized charges of the negative sulfate groups of the heparin function as nucleation points within the gel for the PEDOT polymer. Figure 26a shows a schematic representation of the IPN. The IPN was synthesized on Pt macroelectrodes (diameter 0,5cm) using 2% heparin-MA and 18% PVA-MA. Later in 2014, the group revisited the technique to functionalize Pt electrodes (diameter 1cm) with a CHG functionalized with sericin and gelatin (Figure 26b).

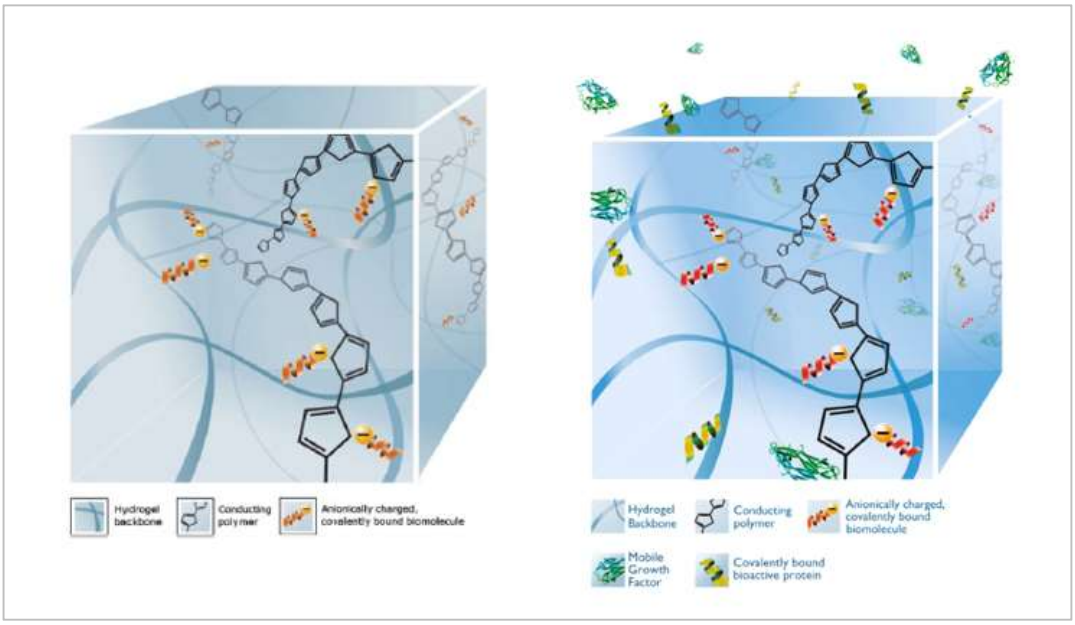

Figure 26 Artistic impression of interpenetrated network with and without functionalization (Figures reproduced from [46, 54] respectively)

To create a CHG for this research PVA-MA was prepared as described earlier. To incorporate nucleation sites inside the HG, Heparin will be crosslinked with the PVA macromers through photopolymerization. To prepare photopolymerizable Heparin macromers, Heparin-MA was prepared based on a protocol from Benoit et al (2005).[55] A 2% heparin in water solution was prepared and a fivefold molar excess of methacrylic anhydride was added. The pH was adjusted to 8,5 using NaOH, and the reaction was allowed to proceed overnight in an ice bath. The polymer was precipitated in acetone and redissolved in water. The sample was then lyophilized and stored for later use.

For HG formation, 0,1% Irgacure 2959 was left to dissolve in water overnight in a 40°C incubation chamber, and vortexed until dissolved. 18% of the lyophilized PVA-MA was added and dissolved at 80°C. 2% of the Heparin-MA was added and vortexed until dissolved. The mixture was then deposited onto the PCB pads using a micro pipet and photo-crosslinked for 30 min and left to dry. Next, the HGs were rehydrated and the PCB pads were immersed in EDOT solution and electrodeposition was performed as described earlier.

PVA/Hep HG was deposited on the first seven pads, PEDOT was deposited as described on pads 1, 4, 6, 8, 10, 12, and 14 (see Figure 27). Impedance measurements show that impedance increased where HG was deposited, but after electrodeposition dropped to levels comparable to those of electrodes where no HG was deposited. However, to determine if a true IPN was formed, the CHG samples should be dried and SEM pictures should be taken to analyze surface morphology.[46]

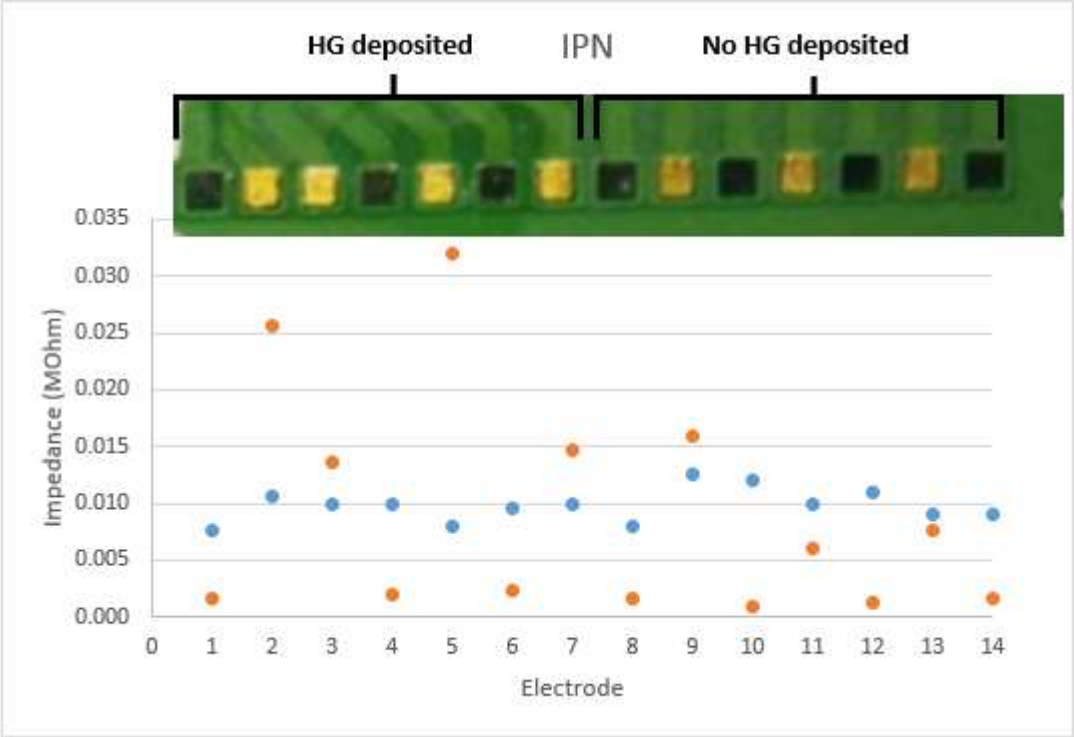

Figure 27 IPN deposition impedance results before (Blue) and after (orange) coating treatment. Electrodes 1, 4, and 6 were coated with HG and coated with PEDOT; Electrodes 2,3,5, and 7 were coated with HG; Electrodes 8, 10, 12, and 14 were coated with PEDOT and Electrodes 9, 11, and 13 remained uncoated (see appendix F for raw data)

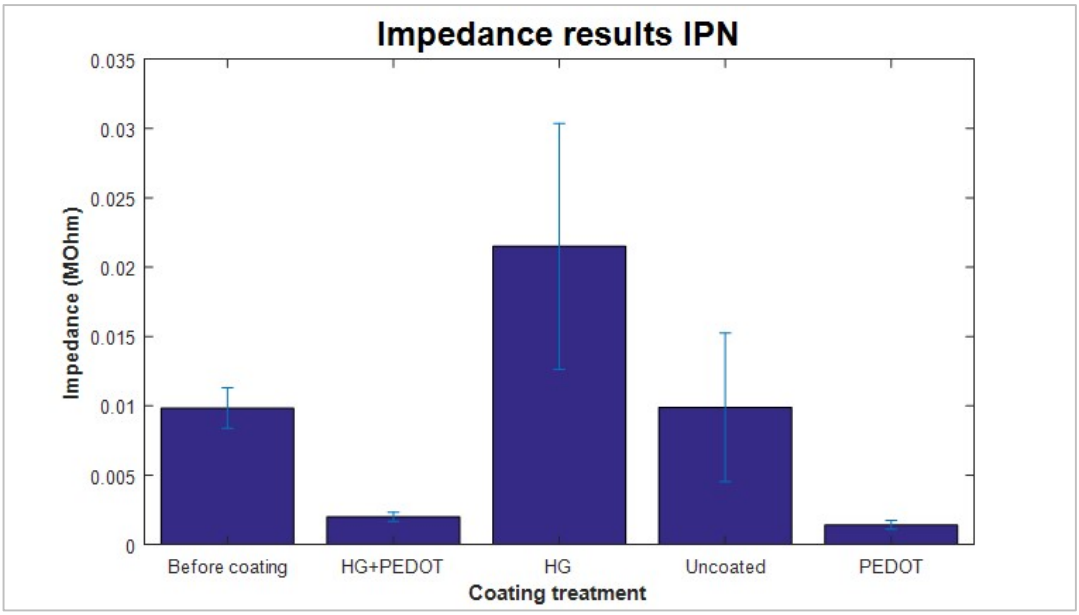

Figure 28 Bar plot Impedance measurements HG + PEDOT coating (The average impedance before coating was found to be significantly different to the average impedance after treatment p<0,05)

4.4 Conclusion

CPs are useful to further reduce the gap between biological tissue and electronics. However, some issues still remain to be overcome. The CP layers tend to have brittle mechanical properties, the Young's modulus remains relatively high, and specificity is not achieved. It is difficult to functionalize a CP layer without influencing other layer properties. A possible way to improve on these issues is the synthesis of CHGs. CHGs have lowered Young's modulus and have high water content, making them an ideal candidate for integration with biological tissue. Furthermore, their macromer chains are available for functionalization, acting as a scaffold to immobilize bioactive molecules. For this research, TiN electrodes were successfully coated with a PEDOT:PSS layer. PVA HGs were successfully synthetized in the form of HG disks and as a layer on top of gold PCB pads, resulting in slightly increased impedance. PVA-Heparin HGs was successfully synthetized and deposited on gold PCB pads, resulting in a slight increase in impedance. A PEDOT layer was successfully coated on top of the gold pads, reducing the impedance

Chapter 5: The interface

The issues associated with long term brain recording and stimulation have resulted in numerous attempts to manipulate and interface with neurons in a stable and controlled way. The approaches that have been explored can broadly be categorized into three main strategies. There is use of topological cues by carefully designing device architecture into well controlled geometries down to the nanoscale. There is use of biomolecules and/or coatings to improve cell adhesion and guidance. And there are biohybrid devices, in which cellular grafts are incorporated to replenish the local neuron population. Using biomimetic materials for developing microsystems that attempt to control neural cell growth and/or elicit a specific cellular response is becoming a research field of high interest. Combining complex biomolecules with nanostructured surfaces is a delicate and costly pursuit, but the potential this combination holds drives the field forward. Of the three approaches described earlier, the use of biomolecules to guide neurons is most widely explored. It has the advantage of interacting with neurons without the difficulties associated with using biohybrid devices.[56]

5.1 State of the art

Numerous studies have attempted to increase cellular adhesion to surfaces by using combinations of coatings and biomolecules.[29] Providing an exhaustive list of these approaches here would not contribute much to the discussion, because the goal here is to create specific, molecularly defined synapse-like structures between neurons and electrodes. To the author's knowledge, no such attempt has been described yet in literature. However, it can be useful to review some papers that reflect the evolution the field has undergone and the current state of the art. Special consideration will be given to work that has dealt with active synapse formation, and use of synaptogenic proteins NLGN-1 and/or LRRTM2.

One of the first studies to focus on active synapse formation in the neuron-to-electrode junction was performed by Bieberich and Guiseppi-Elie in 2004.[57] They were able to induce synapse like connections with neurons on interdigitated MEAs by incubation with neuronal growth factor (NGF) and forskolin, or by serum deprivation and treatment with basic fibroblast growth factor (FGF-2). The interdigitated electrodes were made from Au, Pt or Indium Tin Oxide (ITO). Extensive neurite outgrowth was found, more than on standard tissue culture plastic. Different neurite growth patterns were observed depending on electrode material. Cultures grown on Pt electrodes formed cable like neurites, whereas cultures grown on Au or ITO electrodes showed network like neurite structures. Figure 29 shows fluorescent microscopy results of fully differentiated neurons and working synapse like structures observed after seven days post seeding on ITO electrodes.[57]

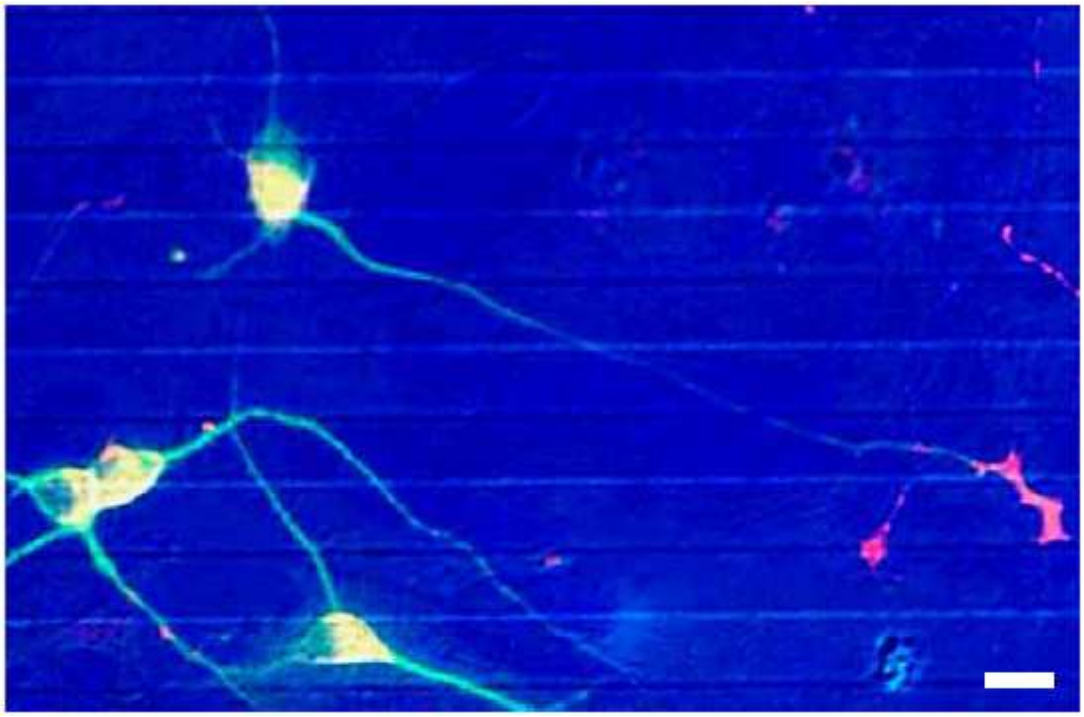

Figure 29 Fluorescent microscopy image of microtubule associated protein-2 (MAP-2, green) shows neurons cultured on top of the interdigitated electrodes and synaptophysin (red) shows active synapse formation sites (Figure reproduced from [57]) (scale bar 10µm)

Some years later Jun et al. (2006) [58] patterned neural networks using microcontact printing (µCP). Patterns of Poly-L-lysin (PLL) were printed on top of a MEA (see Figure 30). Neurites originating from cultured neurons on electrodes grow preferentially on the patterned PLL. The resulting network of neurons allowed to monitor behaviour of neurons structured in neural networks. Fluorescent microscopy revealed synapse formation between neurons close to the soma. However, the connections between the soma (which are only at the electrode sites) were found to be more complicated than cytochemistry tests suggested. Using SEM, it was found that the connections consisted of multiple bundles of neurites, originating from several different neurons. Therefore, it was difficult to determine the role of a single neuron in the network. It is however a nice demonstration of how neurite growth can be manipulated.

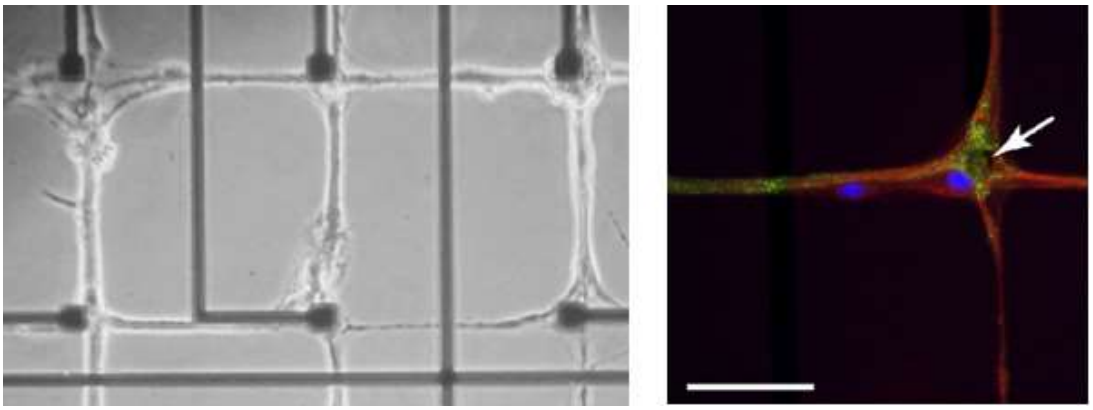

Figure 30 Neurite guidance and synapse staining by Jun et al. LEFT: Phase micrograph of the produced neural network RIGHT: Fluorescence micrograph of neurons near a network node (RED: MAP-2; GREEN: synaptophysin; BLUE: DAPI (4',6-diamidino-2-phenylindole))(scale bar 50µM) (Figures reproduced from [58])

As mentioned before, expression of synaptogenic proteins on non-neuronal cells or beads can induce synapse formation. Moreover, the synapse formation is specific to the subpopulation targeted by the specific synaptogenic protein isoform used in the interface.[17] Czöndör et al. (2013) used synaptogenic proteins to induce synapse formation in a predetermined pattern. By coating synaptogenic proteins on microspheres (diameter 1,5µm) patterned on a non-adhesive surface they developed a method to induce targeted and selective formation of hemisynapses. They found that they could induce synapse formation in dendrites by coating neurexin1-β, resulting in a network of dendrites resembling a subway network (Figure 31). However, when attempting to reverse the system to induce presynapses by coating neuroligin, they found that they were unable to do so, contrary to what has been reported with co-cultures and lipid coated beads. They suggested a number of reasons as to why this may be. For one they suggest that neuronal adhesion dependent solely by axons is much weaker than somato-dendric adhesion. Further, purified neuroligin might be weaker than neurexin and may not survive the 37°C incubation process. Additionally, neuroligin only induces presynaptic differentiation when it is freely diffusible in lipid membranes, and not when immobilized on a substrate as in the study. And, last but not least, neuroligin is assembled as a dimer through interaction between extracellular AchE-like domains, and may not function properly as a monomer[59]. The latter two reasons are connected in the sense that neuroligin monomers that are freely diffusible in lipid membranes are free to form dimers. This suggests that immobilization of neuroligin monomers should be performed in such a way that dimerization is possible (for example multiple adhesion sites of streptavidin).

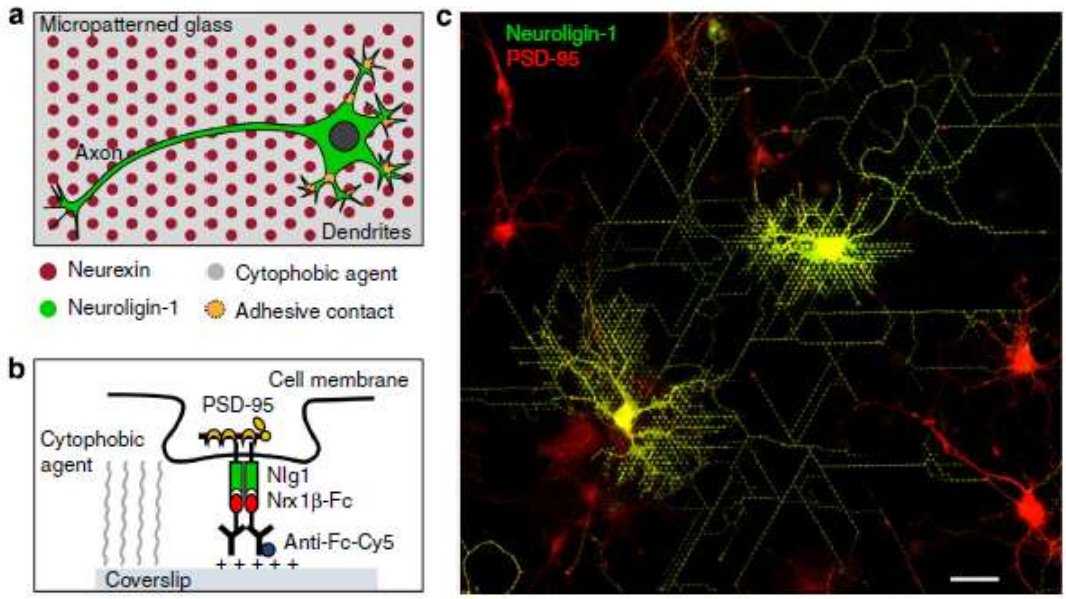

Figure 31 a) schematic of the patterned surface with a cultured neuron. b) schematic of the neurexin-neuroligin connection complex. C) Fluorescence micrograph of neuron proliferation on the nanopatterned neurexin structure (scale bar 5µm) (Figure reproduced from [59])

Kim et al. (2016) [60] were able to induce stable excitatory synapses based on the action of NLGN1 without the need for a suspended lipid bilayer. Using genetic engineering, the NLGN1 ectodomain was attached to a biotin acceptor and a fluorescent marker. The proteins were attached to either Poly-D-lysine (PDK) microbeads, suspended lipid bilayer (SLB) microbeads or streptavidin covered microbeads (dyna). PDK promotes adhesion, but is not specific to excitatory synapses like NLGN1. Synapsin 1 (Syn1) and Bassoon (Bsn) aggregation was measured through mean fluorescence intensity (MFI) (Figure 32). Syn1 and Bsn are general synapse marker proteins associated with synaptogenic activity. The MFI of the synapse marker proteins are an indication of synaptogenic activity. The NLGN1 coated dynabeads showed significantly higher synaptogenic activity. Figure 33 shows the microfluidic device that was used to separate the neuronal cell bodies from the artificial dendrites. Tau staining was used to visualize the neurons cell bodies and neurite outgrowth.

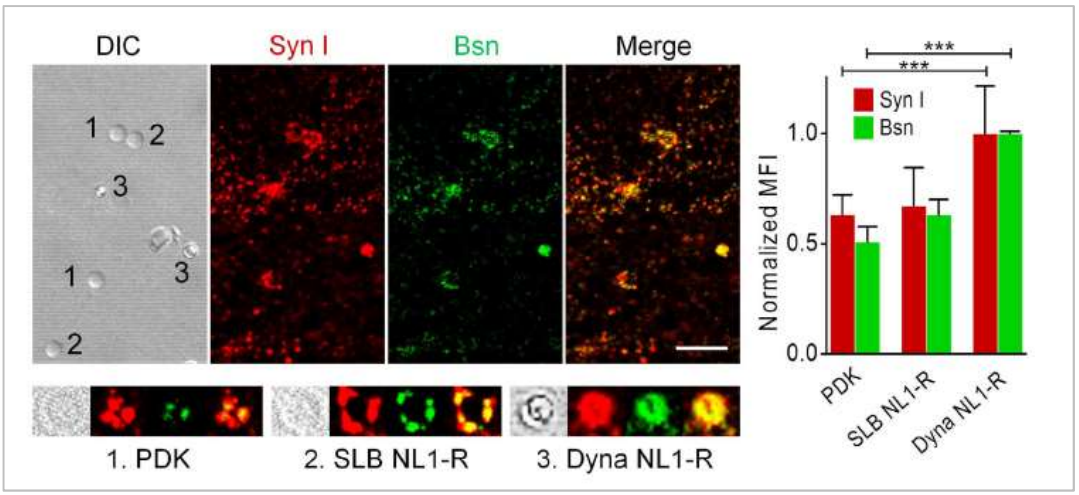

Figure 32 MFI results of Syn1 and Bsn on PDK, SLB or dyna beads. The PDK and NLGN1 coated SLB beads show about the same synaptogenic activity. The NLGN1 coated dyna beads show significantly higher synaptogenic activity. (Scale bar 10 micrometer, ***p < 0.001) (Figure reproduced from [60])

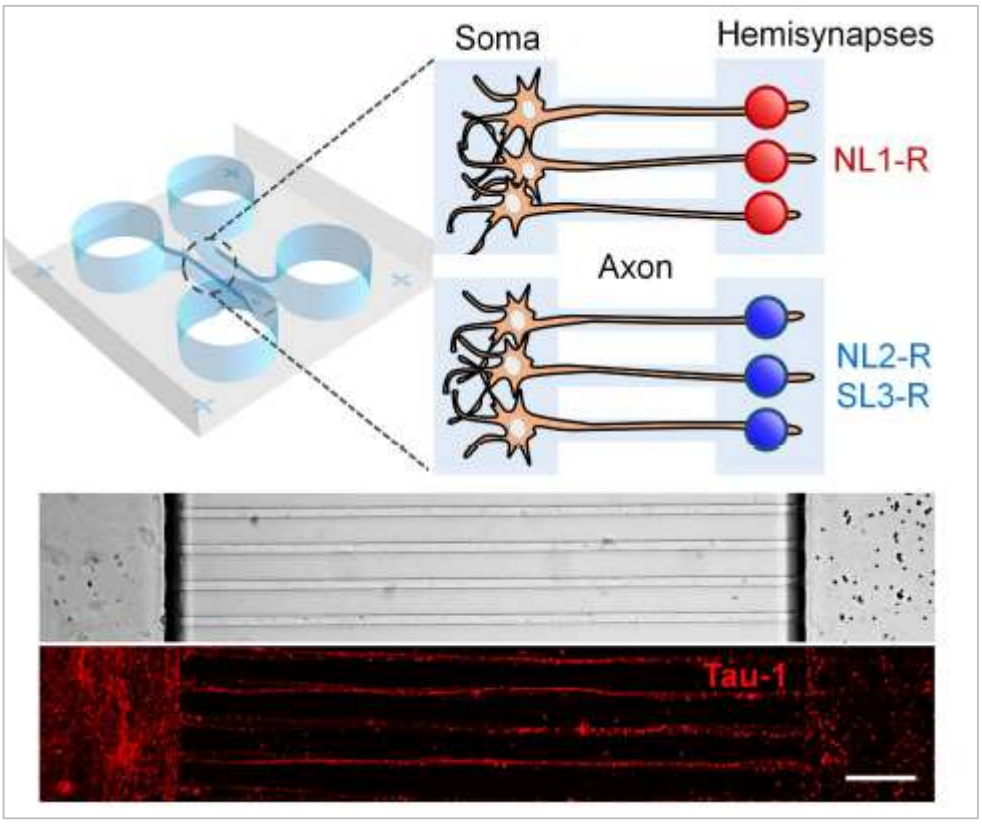

Figure 33 TOP: Schematics of the used microfluidic culture chamber to separate neurons from the artificial dendrites. A glutamate sensor (not shown) was used to determine if the hemisynapses were excitatory synapses. MIDDLE: phase contrast of the microfluidic channels BOTTOM: Tau staining was used to visualise neurons and neurites. (scale bar 20µm) (Figure reproduced from [60])

5.2 The synaptoprobe

As mentioned earlier, plenty of papers describe approaches to manipulate neural morphology and/or neurite growth. There have also been numerous papers describing the use of synaptogenic proteins to induce specific synapse formation.[20, 24, 27, 59] However, combination of specific synapse formation on functionalized electrode surfaces has not been described. The combination of these functionalities into one device is not trivial. Some difficulties are the orientation of the synaptogenic proteins on the surface and the influence of concentration, grouping and dimerization on their functionality. Also, there is a large scale difference between synapse area and electrode area, making it virtually impossible to have a one to one ratio. However, perhaps because synaptic currents/potentials are very low, the prospect of forming multiple hemi-synapses on one electrode site might prove helpful. The synaptic currents are low because the communication in chemical synapses occurs via neurotransmitters, and the current we hope to measure originates from ion fluxes associated with neurotransmitter release.

It is important to overcome these difficulties to develop a tool that could prove extremely useful in neuroscience. This tool, which is called the synaptoprobe here, is a probe with electrodes that have a functionalized coating capable of forming hemi-synapses with targeted subpopulations of neurons. The concept is schematically visualized on Figure 34. Where conventional probes measure APs of all neurons by picking up the larger soma depolarization, the synaptoprobe makes a very close (synapse sized see Figure 35) connection with a subpopulation of neurons that is targeted through synaptogenic proteins. Ideally, the synaptoprobe would only measure firing activity of the targeted population, allowing neuroscientists to selectively listen in to brain activity.

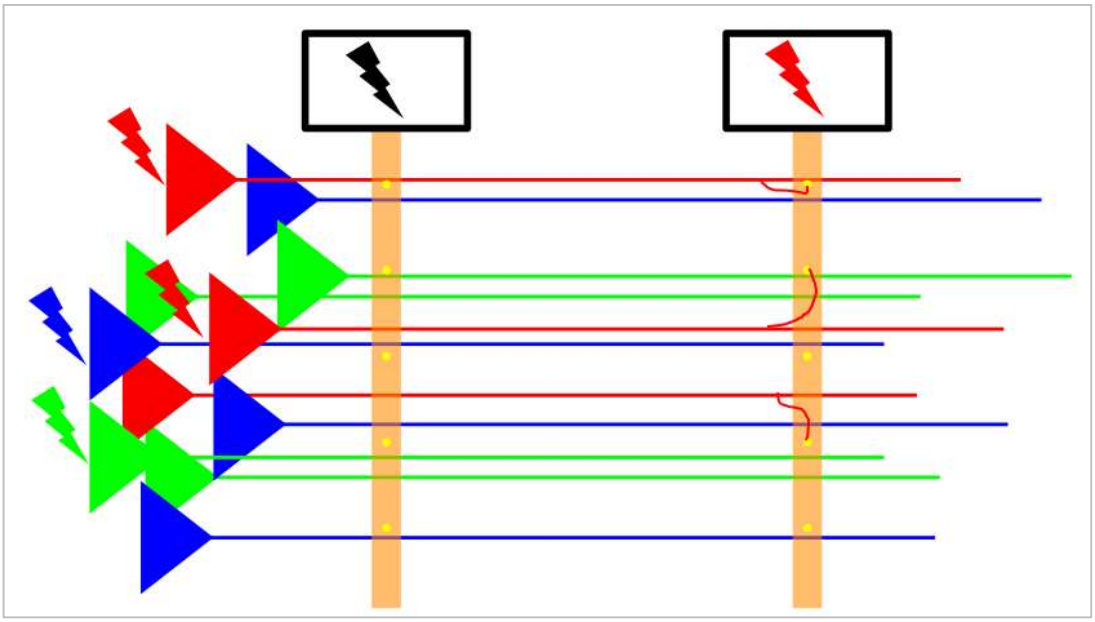

Figure 34 The synaptoprobe concept schematically

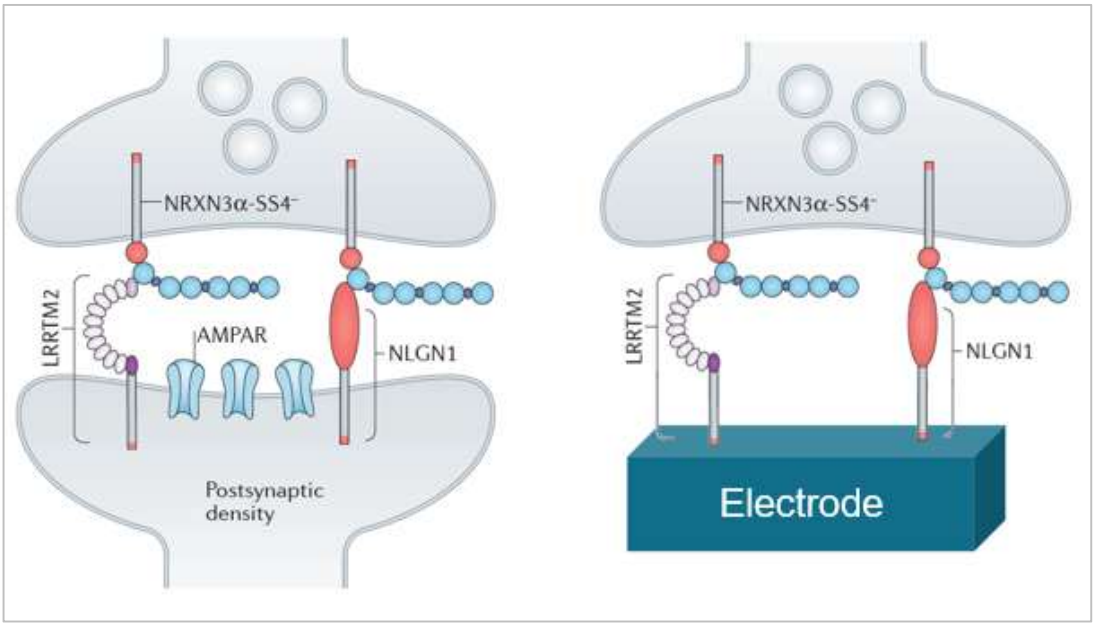

Figure 35 Synaptoprobe electrode concept schematically

As described in the previous chapters, because TiN electrode geometry can be manufactured in small dimensions with relatively low increase of impedance as compared to other materials, they were the material of choice. To functionalize these TiN electrodes modified PVA was chosen because of good biocompatibility and functionalization options. Also PVA can be permeated with conductive polymers to make a CHG, further decreasing impedance. The schematics of the electrode coated with functionalized CHG can be seen on Figure 36. To immobilize synaptogenic proteins onto the PVA HG, two approaches were investigated to functionalize PVA with streptavidin. Because the synaptogenic proteins provided to us had a biotin tagged tail, it was decided to exploit the biotin-streptavidin bonding chemistry to make a stable, but generic system applicable to all compounds with a biotin tail.

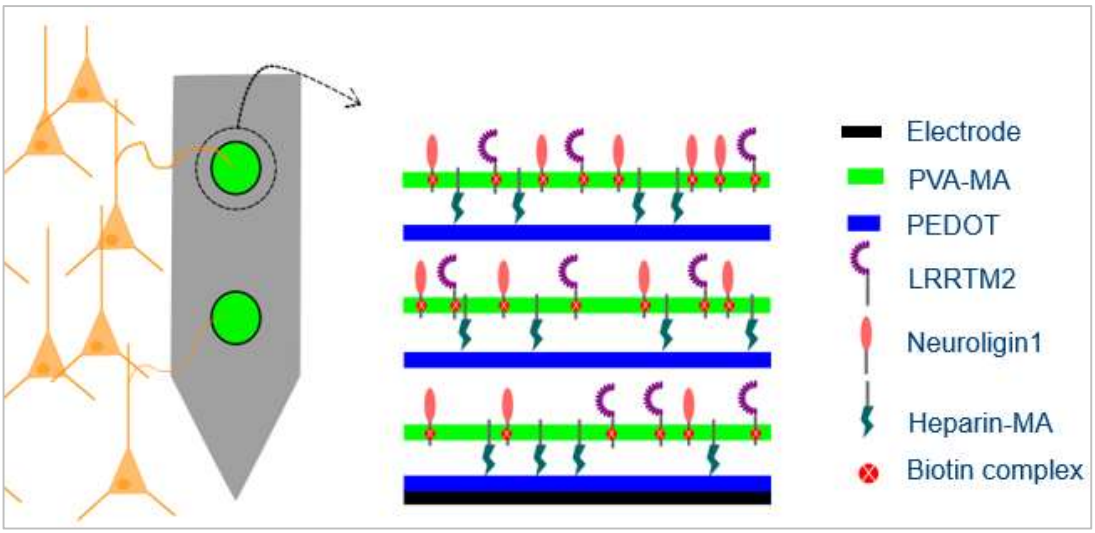

Figure 36 Synaptoprobe electrode structure

The first approach was to use a sandwich structure of PVA-Biotin-streptavidin-Biotin-protein. Here, biotin was covalently grafted directly onto PVA through an esterification reaction (Figure 37). A 5% freeze-dried PVA-MA solution in water was prepared. A 1:20 ratio of repeating monomer/biotin was added and the solution was brought to a pH of 1,5 with HCl. The reaction proceeded overnight at 70°C while stirring. The macromers were then precipitated in acetone and then re-dissolved in water. Dialysis was performed with a 15kDa cut-off membrane to purify the macromers for lyophilization. The HGs were then made in molds as described earlier. The resulting HG discs were first washed in water and then in MES buffer, before incubating in a Avidin-Texas red conjugate for 30 minutes at room temperature. After incubation, the HGs were washed in MES buffer, then in a glycin buffer and then in MES buffer once more. As a control, a preformed HG disc synthetized from a unbiotinylated PVA-MA monomers was also incubated with Avidin-Texas red conjugate using the same washing and incubating steps.

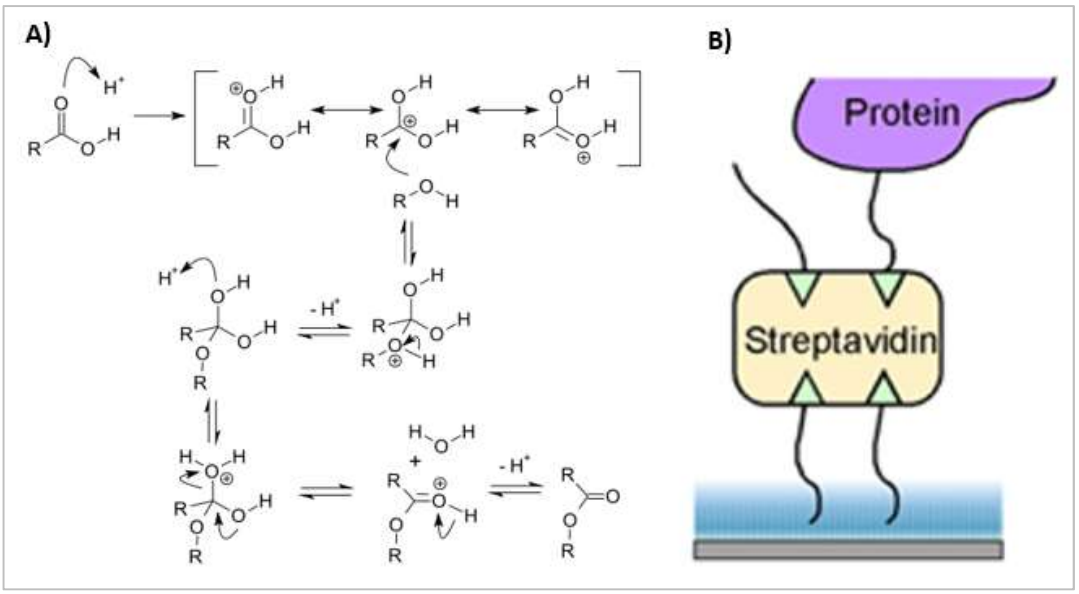

Figure 37 A) Esterification reaction (Figure reproduced from [10]) B) Sandwich model schematic (Figure reproduced from [61])

However, there was concern that the harsh reaction conditions might destroy the biotin molecule. Furthermore, the biotin molecule is small compared to the PVA macromers, and the streptavidin binding cleft for biotin is relatively deep. Therefore, steric hindrance might prevent efficient occupation of streptavidin by biotin molecules. This reaction was also not described in literature, so results were unpredictable. In anticipation of these problems, a second approach was developed prior to testing. In this second approach, as described by Nuttelman et al. (2001)[62], streptavidin is grafted covalently via a 11-bromodecanoic acid (11-BUDA) linker onto the PVA macromolecules (Figure 38). The covalently bound carboxyl functions are then used to perform EDC/NHS coupling of streptavidin (Figure 39), a well-established technique to immobilize proteins onto surfaces.[63]

For the first step, preformed HG discs were added to 10ml of a 3M solution of NaOH. Then 100mg of 11-BUDA was added and left to react for two hours while stirring at 37°C. The HG discs were then removed from the solution and washed thoroughly with water. In the second step, the HG discs were first washed with MES buffer and then activated in EDC/NHS buffer for 15 minutes. The discs were then incubated in a Avidin-Texas red conjugate solution for 30 minutes at room temperature. After incubation the discs were washed in MES buffer, then in a glycin buffer, and finally in MES buffer once more. As a control, a preformed HG disc was treated the same way, only the first step was not preformed.

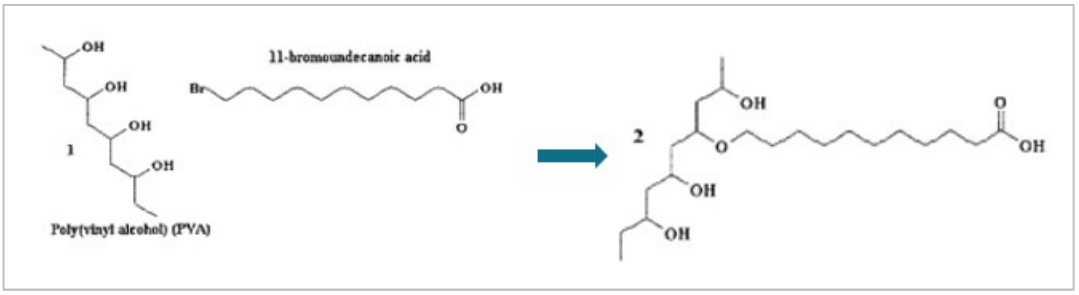

Figure 38 Covalent bonding of 11-BUA to PVA macromers (Adapted from [62])

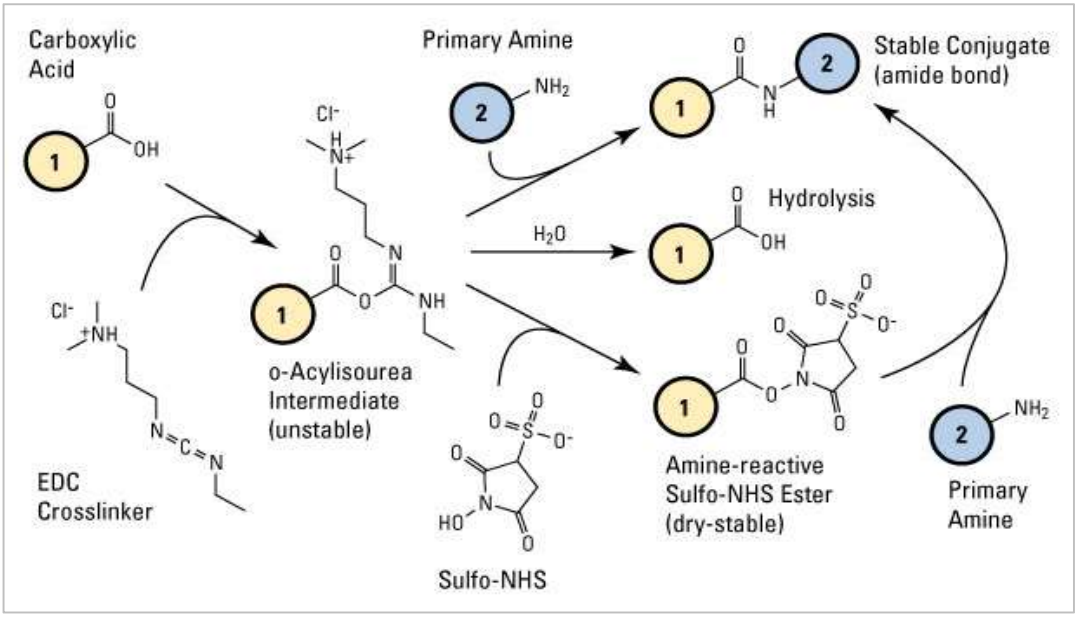

Figure 39 EDC/NHS coupling (Figure reproduced from [63])

Fluorescent confocal microscopy was used to determine if the avidin-Texas red conjugate was successfully bound to the PVA hydrogels, using the parameters listed in table 1.

Table 1 Fluorescent microscopy parameters

Microscope	*LSM 710, Axio Examiner*
Objective	EC Plan-Neofluar 5x/0.16 M27
Pinhole	57 µm
Excitation wavelength	561 nm
Emission wavelength	628 nm
Airy unit	1
Digital off	1
Scan time	22,45
Section	49,2
Gain	949
Laser Power	• Samples: 10 • Blanks: 100

Hydrogels were placed between two glass slides and compressed to make the top surface flat. The resulting pictures are shown on Figure 40. The pictures are recorded in greyscale, with greyscale intensity per pixel varying with fluorescence intensity. The greyscale pictures are then colored in red to enhance visibility. Mean fluorescent intensity (MFI) of the top ten percentile of the highest intensity pixels were calculated (Figure 41, for calculations see matlab script appendix G).

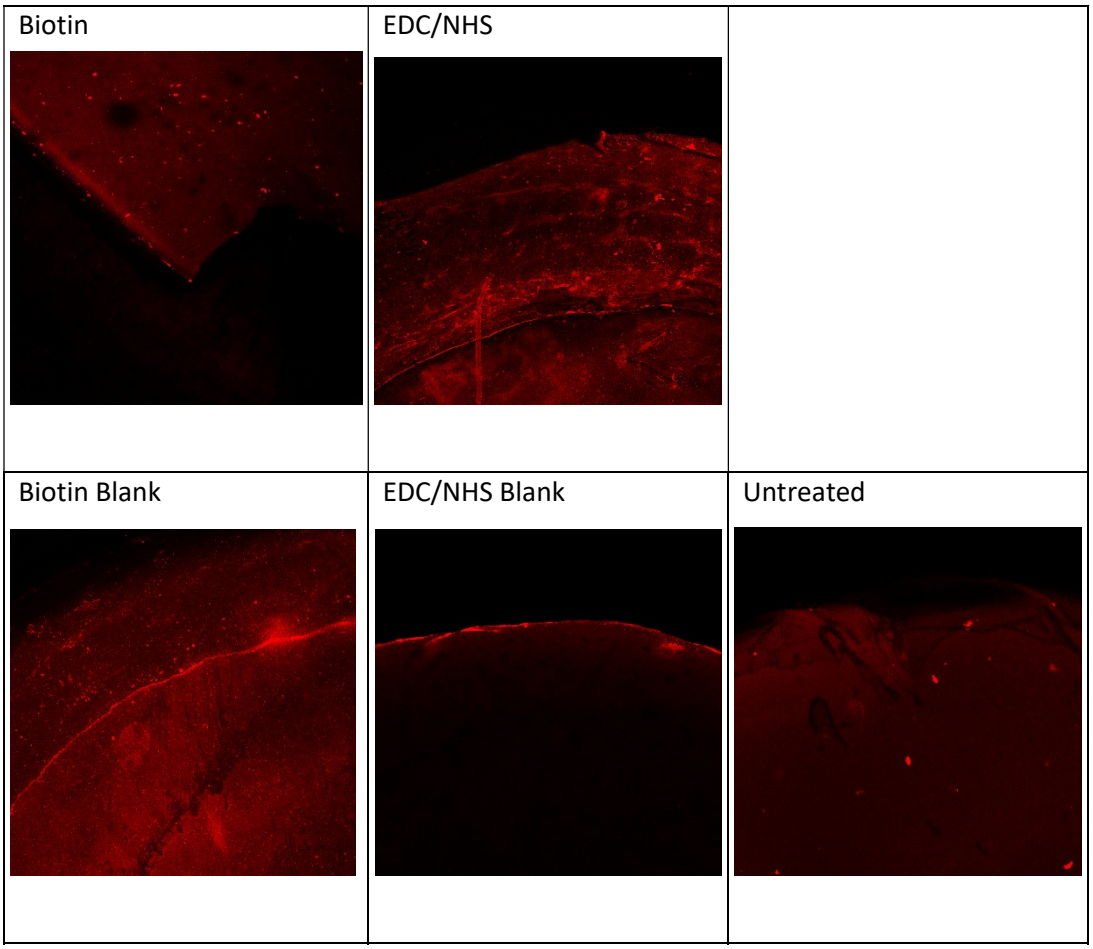

Figure 40 Fluorescent confocal microscopy results TopLeft: HG disc synthetized from biotin conjugated PVA-MA, incubated with avidin TopMiddle: HG disc functionalized with 11-BUDA, then EDC/NHS coupled avidin BottomLeft: HG disc synthetized from PVA-MA, incubated with avidin BottomMiddle: HG disc EDC/NHS coupled with avidin (this picture was taken from a non-compressed HG disk) BottomRight: Untreated HG disc

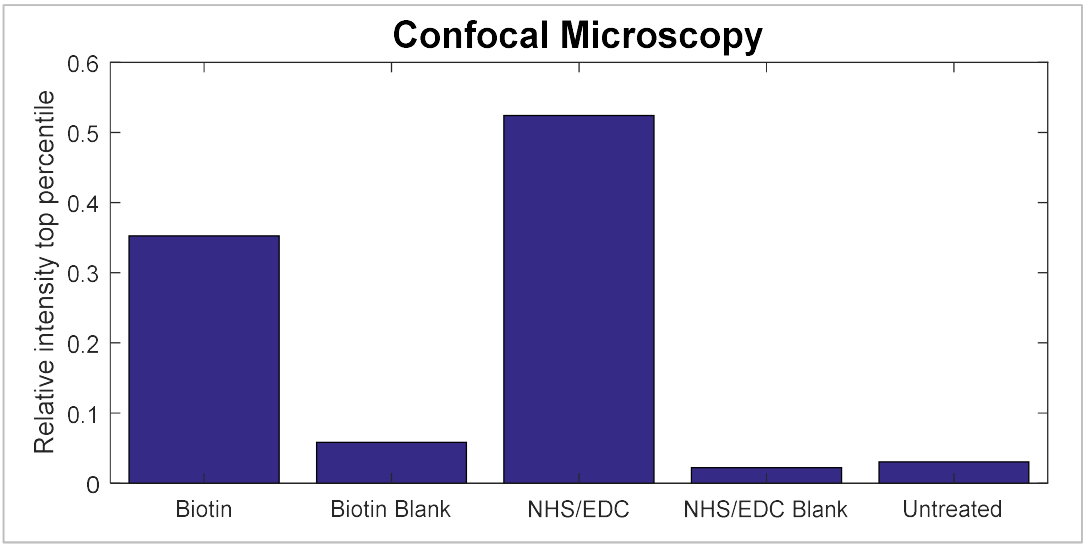

Figure 41 Fluorescent confocal microscope MFI top ten percentiles (for calculation see matlab script in appendix G)

5.3 Conclusion

Much research has been done in the pursuit to link biological and synthetic materials. Much of this research however, is restricted to a-specifically increasing affinity of biological material to synthetic surfaces. Other research pursues specific binding, using Neuroligin1 and LRRTM2 to induce specific synapse formation. However, no research has combined the use of these synaptogenic proteins with electrode surface modification to attempt specific trans-synaptic AP recording, which could be a very valuable tool for neuroscience. To link biotin tagged synaptogenic proteins onto PVA macromers, PVA was functionalized with streptavidin through two different pathways. It was shown that both approaches succeeded to bind streptavidin, suggesting they are ready to be functionalized with biotin tagged proteins.

Chapter 6: Conclusion

The field of brain machine interfacing is getting more and more attention for a variety of applications. However, it remains a relatively new field, with many scientific hurdles left to be taken. One of the major scientific hurdles is the foreign body response of the brain tissue. It seems that using biomolecules in the brain machine interface is a promising approach to modulate the foreign body response. Choosing materials with good biocompatibility properties is also a good choice for brain machine interfacing.

In this work a design is proposed to functionalize electrodes with bio-functionalized materials to make a specific brain machine interface capable of selective action potential measurement. The materials were chosen after careful review of current literature. The protocols and chemistry were performed and found to be feasible. However, interaction with live neurons was not studied, thus it is not possible to make any conclusions on whether or not this design will be functional. It is clear that much work remains to be done. As the research stands now, the next step would be to investigate interaction with neurons, and preferably with neurites, specifically axon terminals. A possible way to do this is to create a microfluidic PDMS stamp with channels through which neurites can grow. Further characterization of functionalized HGs would also be useful. Furthermore other HGs (for example, alginate) may be considered, and different ways of making CHGs (for example with covalently bound taurine[54]). Also thought must be given to patterning and scaling issues (photo-initiators/micro- and nanogels). And the possibility must be explored to design devices entirely made out of HGs (additive HG design using different HGs in one device).

It seems clear though, that the HG/biofunctionalization combination is promising in its diversity and adaptability. The large interest in tissue engineering is a testimony to that. Many of the problems faced in tissue engineering are in essence the same as those in brain machine interfacing, thus it is no surprise that the answers are sought in the same direction.

In future research to this master's thesis, further characterization is needed of the HGs and CHGs using NMR, XPS, and SEM to determine chemical composition and corresponding morphology, also Young's modulus should be determined and further conductivity studies are needed. Furthermore, repeatability of the protocols needs to be tested and optimized. In vitro testing is also needed to determine if the approach works, and what exactly can be measured. Further down the road, the possibility of adding extra functionality to the CHGs can be explored (for example incorporation of NGF or other bioactive molecules) and neuron stimulation methods (electrical or biochemical by neurotransmitter incorporation[64])

Appendices

Appendix A: Electrode configuration

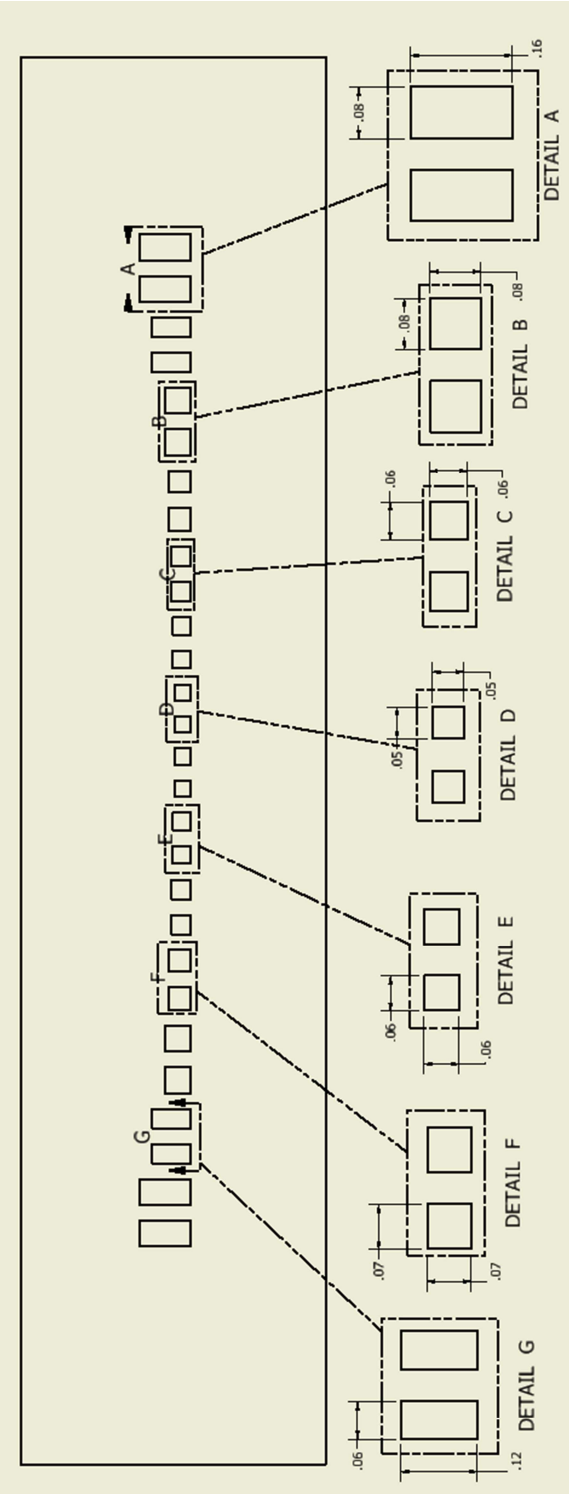

Figure 42 Electrode configuration and geometry (mm)

Electrodes	Surface (mm^2)
A	1,280E-4
B	6,400E-5
C	3,600E-5
D	2,500E-5
E	3,025E-5
F	4,900E-5
G	7,200E-5

Table 2 Electrode surface area

Appendix B: PCB design

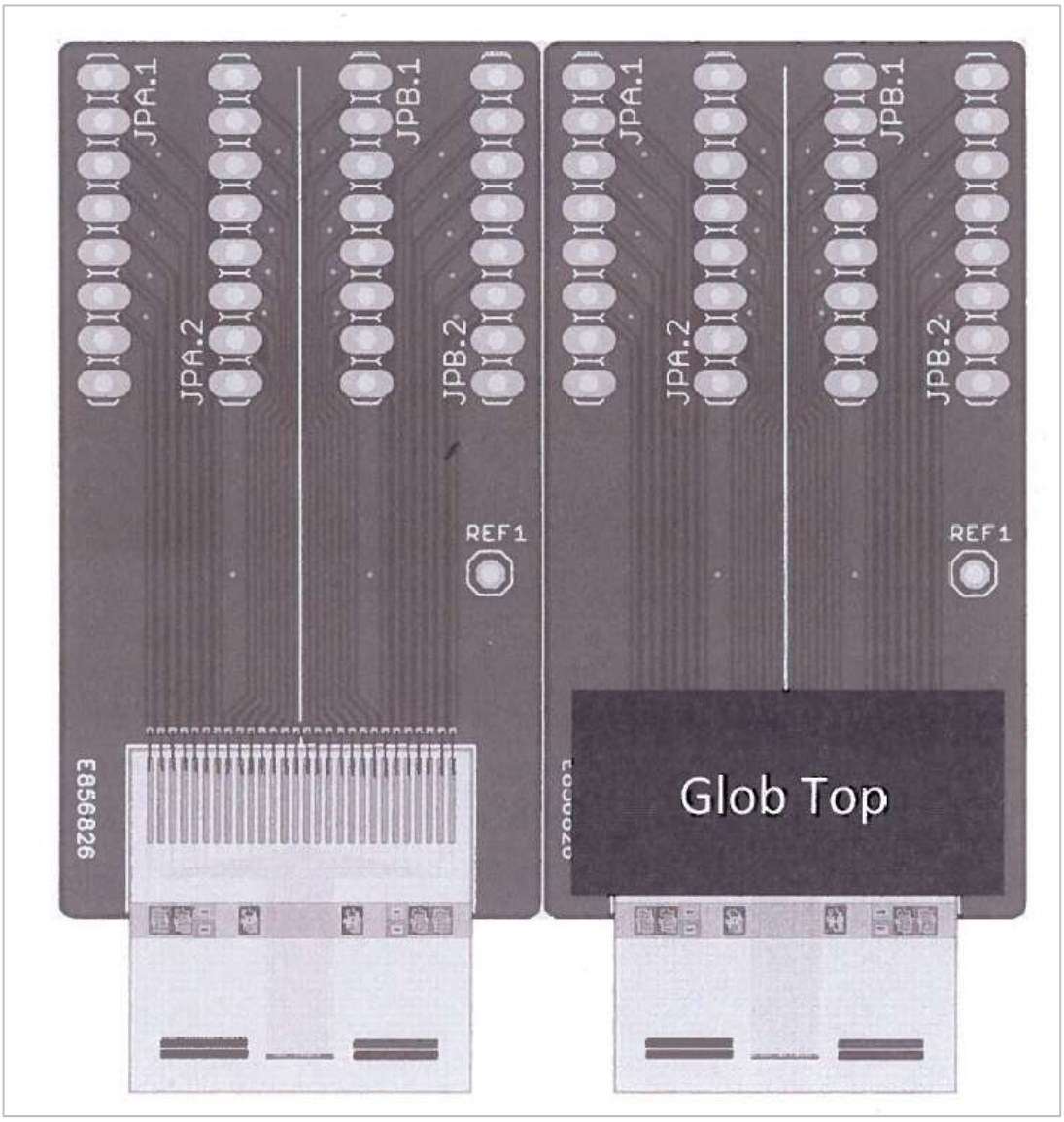

Figure 43 PCB design

Appendix C: NanoZ channel mapping

```
;-----------------------------------------------------------

[Synaptoprobe_left]
Name              = Synaptoprobe_left
Description = left 7 pair electrodes
SiteSizeX   = 23
SiteSizeY   = 23
RoundSite   = 0

;define electrode outline
;format is "Outline_ = x, y" (in microns)
NumPoints = 6

Outline0  = -1000, 0
Outline1  = 1000, 0
Outline2  = 1000, 500
Outline3  = -1000, 500
Outline4  = -1000, 0
Outline5  = -1000, 0

;define electrode sites
;format is "Site _ = x, y, sizeX[optional], sizeY[optional]"
NumSites  = 16

Site 0 = -999, 0
Site 0 = -999, 0
Site 1  = -950, 250, 50, 100
Site 2  = -820, 250, 50, 100
Site 3  = -690, 250, 50, 75
Site 4  = -560, 250, 50, 75
Site 5  = -430, 250, 50, 50
Site 6  = -300, 250, 50, 50
Site 14  = 740, 250, 30, 30
Site 13 = 610, 250, 30, 30
Site 12 = 480, 250, 35, 35
Site 11 = 350, 250, 35, 35
Site 10 = 220, 250, 40, 40
Site 9 = 90, 250, 40, 40
Site 8 = -40, 250, 45, 45
Site 7 = -170, 250, 45, 45
```

```
;-------------------------------------------------------

[Synaptoprobe_right]
Name              = Synaptoprobe_right
Description = Right 7 pair electrodes
SiteSizeX   = 23
SiteSizeY   = 23
RoundSite   = 0

;define electrode outline
;format is "Outline_ = x, y" (in microns)
NumPoints = 6

Outline0  = -1000, 0
Outline1  = 1000, 0
Outline2  = 1000, 500
Outline3  = -1000, 500
Outline4  = -1000, 0
Outline5  = -1000, 0

;define electrode sites
;format is "Site _ = x, y, sizeX[optional], sizeY[optional]"
NumSites  = 14

Site 7  = -40, 250, 45, 45
Site 8  = -170, 250, 45, 45
Site 9  = -300, 250, 40, 40
Site 10  = -430, 250, 40, 40
Site 11  = -560, 250, 35, 35
Site 12  = -690, 250, 35, 35
Site 13  = -820, 250, 30, 30
Site 14 = -950, 250, 30, 30
Site 6 = 90, 250, 50, 50
Site 5 = 220, 250, 50, 50
Site 4 = 350, 250, 50, 75
Site 3 = 480, 250, 50, 75
Site 2 = 610, 250, 50, 100
Site 1 = 740, 250, 50, 100
```

Appendix D: Impedance measurements

Sonification	*Impedance (Mohm)*				
Electrode	Rep 1	Rep 2	Rep 3	Average	Stdev
1	0.01	0.011	0.01	0.010	0.001
2	0.011	0.011	0.011	0.011	0.000
3	0.028	0.028	0.028	0.028	0.000
4	0.025	0.025	0.025	0.025	0.000
5	0.026	0.026	0.026	0.026	0.000
6	56.682	53.346	57.996	56.008	2.397
7	0.044	0.044	0.044	0.044	0.000
8	0.042	0.042	0.042	0.042	0.000
9	0.093	0.094	0.093	0.093	0.001
10	0.09	0.09	0.09	0.090	0.000
11	0.137	0.139	0.139	0.138	0.001
12	0.19	0.197	0.199	0.195	0.005
13	0.218	0.223	0.224	0.222	0.003
14	0.249	0.257	0.258	0.255	0.005
15	0.259	0.263	0.264	0.262	0.003
16	0.242	0.245	0.245	0.244	0.002
17	0.112	0.113	0.113	0.113	0.001
18	0.113	0.115	0.115	0.114	0.001
19	0.072	0.071	0.072	0.072	0.001
20	0.077	0.078	0.078	0.078	0.001
21	0.033	0.033	0.033	0.033	0.000
22	0.037	0.037	0.037	0.037	0.000
23	0.02	0.02	0.02	0.020	0.000
24	0.02	0.02	0.02	0.020	0.000
25	0.017	0.018	0.018	0.018	0.001
26	84.128	83.246	85.966	84.447	1.388
27	0.008	0.008	0.008	0.008	0.000
28	0.008	0.009	0.008	0.008	0.001

Table 3 Initial impedance measurements after sonication

H2O rinse	*Impedance (Mohm)*				
Electrode	Rep 1	Rep 2	Rep 3	Average	Stdev
1	0.007	0.007	0.007	0.007	0.000
2	0.007	0.007	0.007	0.007	0.000
3	0.014	0.014	0.014	0.014	0.000
4	0.013	0.014	0.013	0.013	0.001
5	0.015	0.015	0.014	0.015	0.001
6	56.029	54.373	58.211	56.204	1.925
7	0.021	0.021	0.02	0.021	0.001
8	0.02	0.02	0.02	0.020	0.000
9	0.032	0.032	0.032	0.032	0.000
10	0.032	0.032	0.032	0.032	0.000
11	0.043	0.043	0.042	0.043	0.001
12	0.042	0.041	0.041	0.041	0.001
13	0.056	0.056	0.056	0.056	0.000
14	0.058	0.058	0.058	0.058	0.000
15	0.058	0.058	0.058	0.058	0.000
16	0.057	0.058	0.058	0.058	0.001
17	0.04	0.04	0.04	0.040	0.000
18	0.039	0.039	0.039	0.039	0.000
19	0.028	0.028	0.028	0.028	0.000
20	0.028	0.029	0.028	0.028	0.001
21	0.017	0.017	0.017	0.017	0.000
22	0.018	0.017	0.018	0.018	0.001
23	0.012	0.012	0.013	0.012	0.001
24	0.012	0.013	0.012	0.012	0.001
25	0.011	0.011	0.011	0.011	0.000
26	0.011	0.011	0.011	0.011	0.000
27	0.006	0.006	0.006	0.006	0.000
28	0.006	0.006	0.006	0.006	0.000

Table 4 Initial impedance measurements after H2O rinse

IPA rinse	*Impedance (Mohm)*				
Electrode	Rep 1	Rep 2	Rep 3	Average	Stdev
1	0.005	0.005	0.006	0.005	0.001
2	0.005	0.006	0.006	0.006	0.001
3	0.01	0.01	0.01	0.010	0.000
4	0.01	0.01	0.01	0.010	0.000
5	0.011	0.011	0.011	0.011	0.000
6	52.872	55.539	50.548	52.986	2.497
7	0.014	0.015	0.015	0.015	0.001
8	0.014	0.015	0.015	0.015	0.001
9	0.022	0.022	0.022	0.022	0.000
10	0.022	0.022	0.022	0.022	0.000
11	0.028	0.028	0.028	0.028	0.000
12	0.029	0.028	0.028	0.028	0.001
13	0.038	0.038	0.038	0.038	0.000
14	0.039	0.039	0.038	0.039	0.001
15	0.04	0.04	0.04	0.040	0.000
16	0.041	0.04	0.041	0.041	0.001
17	0.029	0.029	0.029	0.029	0.000
18	0.028	0.028	0.029	0.028	0.001
19	0.021	0.021	0.021	0.021	0.000
20	0.022	0.022	0.022	0.022	0.000
21	0.014	0.014	0.014	0.014	0.000
22	0.014	0.014	0.014	0.014	0.000
23	0.01	0.01	0.01	0.010	0.000
24	0.01	0.01	0.01	0.010	0.000
25	0.009	0.009	0.009	0.009	0.000
26	90.746	85.141	78.312	84.733	6.227
27	0.005	0.005	0.005	0.005	0.000
28	0.005	0.005	0.005	0.005	0.000

Table 5 Initial impedance measurements after IPA rinse

Appendix E: Materials and methods

1. Materials

    a. Reagents (all reagents were purchased from Sigma Aldrich unless indicated otherwise)

- PVA macromers: Mowiol® 4-98 ~27000 kDa
- Heparin: Heparin sodium salt from porcine intestinal mucosa; Grade I-A, ≥180 USP units/mg, powder, BioReagent, suitable for cell culture
- EDOT: 3,4-Ethylenedioxythiophene 97%
- PSS: Donated by the LSI group
- pTS: para-toluenesulfonic acid monohydrate; ACS reagent ≥98,5%
- PBS: phosphate buffer salt; generic lab reagent
- Acetone: generic lab reagent
- Methanol: generic lab reagent
- ACN: generic lab reagent
- Biotin: ≥99% (TLC), lyophilized powder
- GMA: glycidyl methacrylate: 97%, contains 100ppm monomethyl ether hydroquinone as inhibitor
- Methacrylic anhydrate: Provided by materials science department
- Streptavidin
- Fluorescent streptavidin
- Irgacure 2959: provided by the biomaterials group at the faculty of material science
- EDC: provided by the chemistry department
- NHS: provided by the chemistry department
- MES: provided by the chemistry department
- Glycin: provided by the chemistry department

    b. other

- Dialysis membrane: 16000 kDa cut off filter membrane. Provided by the biomaterials group at materials science department
- Molds: Provided by the biomaterials group at materials science department. 3D printed at nerf.

    c. Devices

- UV light: Provided by the biomaterials group at materials science department
- Lyophilizer: Provided by the biomaterials group at materials science department
- NMR: Provided by the biomaterials group at the chemistry department
- NanoZ:

- SEM: performed at Imec
- Fluorescent microscope: Performed at Nerf

2. Methods

- Methacrylation:

  For PVA; 5% PVA was made by dissolving 1g PVA in 20ml of water at 80°C. The PVA repeating unit has a MW of 44g/mol ➔ 1g / 44g/mol = 0,023mol. A 1:1 ratio of GMA was added (3ml). pH was adjusted to 1,5 using concentrated HCl. The reaction was then allowed to proceed overnight at 60°C while stirring and protected from light. The reaction was then stopped and the polymer was precipitated in acetone, then re-dissolved in water. The solution was then filtered with a dialysis cut-off filter at 16000kDa. After three days of filtering, the solution was freeze dried, leaving the lyophilized PVA stored for further use.

  For Heparin; 2% Heparin was dissolved in water, a fivefold excess of methacrylic anhydride was added. pH was adjusted to 8,5 using NaOH. The reaction was allowed to proceed overnight while stirred at 4°C. The reaction was then stopped and the polymer was precipitated in acetone, then re-dissolved in water. The solution was then filtered with a dialysis cut-off filter at 16000kDa. After three days of filtering, the solution was freeze dried, leaving the lyophilized Heparin stored for further use.

- Biotinylation

  A 2% PVA-MA solution was prepared. Biotin was added at a 1:20 ration with PVA repeating unit. pH was adjusted to 1,5 using HCl. The reaction was allowed to proceed over night with stirring at 60°C, protected from light. The reaction was then stopped and the polymer was precipitated in acetone, then re-dissolved in water. The solution was then filtered with a dialysis cut-off filter at 16000kDa. After three days of filtering, the solution was freeze dried, leaving the lyophilized PVA-MA-Biotin stored for further use.

- Lyophilization

  The sample was pre-freeze at -40°C. The sample was then transferred to the lyophilization chamber. The lyophilizer was switched on. When the Eutectic temperature was reached, the vacuum pump was switched on. The sample was left to freeze dry for several days, until completely dry.

- NMR

  ^{1}H-NMR was performed on the freeze dried samples (dissolved in D_2O). The results were analyzed with MESTRENOVA software in manual mode.

- Electrodeposition

  EDOT/pTS (0,1M/0,05M) in H_2O/MeOH (1/1) was prepared and stirred thoroughly. The solution was then bubbled through with nitrogen gas to eliminate oxygen from the solution. Electrodeposition was performed at 1mA/cm².

- Photopolymerization

  Irradiation with 365 nm light at room temperature for 15min at least

Appendix F: Impedance measurements IPN

Before	*Impedance (Mohm)*				
Electrode	Rep 1	Rep 2	Rep 3	Average	Stdev.
1	0.008	0.007	0.008	0.008	0.001
2	0.011	0.011	0.01	0.011	0.001
3	0.01	0.01	0.01	0.010	0.000
4	0.01	0.01	0.01	0.010	0.000
5	0.008	0.008	0.008	0.008	0.000
6	0.01	0.01	0.009	0.010	0.001
7	0.01	0.01	0.01	0.010	0.000
8	0.008	0.008	0.008	0.008	0.000
9	0.013	0.013	0.012	0.013	0.001
10	0.012	0.012	0.012	0.012	0.000
11	0.01	0.01	0.01	0.010	0.000
12	0.011	0.011	0.011	0.011	0.000
13	0.009	0.009	0.009	0.009	0.000
14	0.009	0.009	0.009	0.009	0.000

Table 6 Impedance measurement before IPN

After	*Impedance (Mohm)*				
Electrode	Rep 1	Rep 2	Rep 3	Average	Stdev.
1	0.002	0.001	0.002	0.002	0.001
2	0.026	0.026	0.025	0.026	0.001
3	0.014	0.014	0.013	0.014	0.001
4	0.002	0.002	0.002	0.002	0.000
5	0.033	0.032	0.031	0.032	0.001
6	0.002	0.003	0.002	0.002	0.001
7	0.015	0.015	0.014	0.015	0.001
8	0.001	0.002	0.002	0.002	0.001
9	0.016	0.016	0.016	0.016	0.000
10	0.001	0.001	0.001	0.001	0.000
11	0.006	0.006	0.006	0.006	0.000
12	0.002	0.001	0.001	0.001	0.001
13	0.008	0.007	0.008	0.008	0.001
14	0.002	0.001	0.002	0.002	0.001

Table 7 Impedance measurement after IPN

Appendix G: Matlab script MFI

```
%% Open images

Biotin = imread('BiotinBest.tif');
BiotinBlank = imread('BiotinBlank.tif');
NHS = imread('NHS1Best.tif');
NHSBlank = imread('NHSBlankBest.tif');
UltimateBlankSquashed = imread('UltimateBlankSquashedBest.tif');

%% Process images

BiotinNorm = double(Biotin)/255;
BiotinBlankNorm = double(BiotinBlank)/255/10;
NHSNorm = double(NHS)/255;
NHSBlankNorm = double(NHSBlank)/255/10;
UltimateBlankSquashedNorm = double(UltimateBlankSquashed)/255/10;

%% Take Percentiles

BiotinPrc = prctile(BiotinNorm(:),90);
BiotinBlankPrc = prctile(BiotinBlankNorm(:),90);
NHSPrc = prctile(NHSNorm(:),90);
NHSBlankPrc = prctile(NHSBlankNorm(:),90);
UltimateBlankSquashedPrc =
prctile(UltimateBlankSquashedNorm(:),90);

%% Average top ten percentile

BiotinMean = mean(BiotinNorm(BiotinNorm>BiotinPrc));
BiotinBlankMean =
mean(BiotinBlankNorm(BiotinBlankNorm>BiotinBlankPrc));
NHSMean = mean(NHSNorm(NHSNorm>NHSPrc));
NHSBlankMean = mean(NHSBlankNorm(NHSBlankNorm>NHSBlankPrc));
UltimateBlankSquashedMean =
mean(UltimateBlankSquashedNorm(UltimateBlankSquashedNorm>UltimateBl
ankSquashedPrc));


%% Make bar graphs
y = [BiotinMean BiotinBlankMean NHSMean NHSBlankMean
UltimateBlankSquashedMean];
bar (y)
```

Bibliography

[1] T. Urban, "Neuralink and the brain's magical future," in *Wait but why*, ed, 2017.

[2] M. J. Ravosa, *Primate Origins: Adaptations and Evolution* (Developments in Primatology). Boston, MA: Boston, MA : Springer US, 2007.

[3] F. Stanley, *Origins of neuroscience*. USA: Oxford university press, 2001.

[4] WHO, *Neurological disorders: public health challenges*. 2006.

[5] J. S. Reznick, "Beyond war and military medicine: Social factors in the development of prosthetics," (in English), *Archives of Physical Medicine and Rehabilitation,* Article; Proceedings Paper vol. 89, no. 1, pp. 188-193, Jan 2008.

[6] A. C. Clarke, *Profiles of the Future: An Inquiry into the Limits of the Possible*. USA: Phoenix, 1962.

[7] H. Lodish *et al.*, *Molecular cell biology*, 6th ed. ed. New York: New York : Freeman, 2008.

[8] G. Dunn, "Self reflected micro etching," ed, 2017.

[9] F. A. C. Azevedo *et al.*, "Equal Numbers of Neuronal and Nonneuronal Cells Make the Human Brain an Isometrically Scaled-Up Primate Brain," (in English), *Journal of Comparative Neurology,* Article vol. 513, no. 5, pp. 532-541, Apr 2009.

[10] wikipedia.

[11] S. P. Lacour, G. Courtine, and J. Guck, "Materials and technologies for soft implantable neuroprostheses," *Nat. Rev. Mater.,* vol. 1, no. 10, p. 16063.

[12] E. N. D. Nathaniel, "The reactive astrocyte," ed: Academic Press, 1981, pp. 249-301.

[13] E. A. Ling and W. C. Wong, "THE ORIGIN AND NATURE OF RAMIFIED AND AMEBOID MICROGLIA - A HISTORICAL REVIEW AND CURRENT CONCEPTS," (in English), *Glia,* Article vol. 7, no. 1, pp. 9-18, Jan 1993.

[14] N. L. Strominger, *Noback's Human Nervous System, Seventh Edition: Structure and Function*, 7th ed. ed. (Noback''s Human Nervous System, Seventh Edition). Totowa, NJ: Totowa, NJ : Humana Press : Imprint Humana Press, 2012.

[15] T. C. Südhof, "THE SYNAPTIC VESICLE CYCLE," vol. 27, pp. 509-547.

[16] G. M. Shepherd, *The synaptic organization of the brain*, 2nd ed. ed. New York: New York : Oxford university press, 1979.

[17] M. E. Williams, J. de Wit, and A. Ghosh, "Molecular Mechanisms of Synaptic Specificity in Developing Neural Circuits," (in English), *Neuron,* Review vol. 68, no. 1, pp. 9-18, Oct 2010.

[18] A. Dityatev, *Molecular Mechanisms of Synaptogenesis*. Dordrecht: Dordrecht : Springer, 2006.

[19] M. J. Pinto and R. D. Almeida, "Puzzling out presynaptic differentiation," (in English), *Journal of Neurochemistry,* Review vol. 139, no. 6, pp. 921-942, Dec 2016.

[20] T. J. Siddiqui, R. Pancaroglu, Y. Kang, A. Rooyakkers, and A. M. Craig, "LRRTMs and Neuroligins Bind Neurexins with a Differential Code to Cooperate in

Glutamate Synapse Development," (in English), *Journal of Neuroscience,* Article vol. 30, no. 22, pp. 7495-7506, Jun 2010.
[21] C.-H. Y. Yen-Pei Lu, J. Andrew Yeh, Fu Han Ho, Yu-Cheng Ou, Chieh Hsiao Chen, Ming-Yu Lin, Keng-Shiang Huang, "Guidance of neural regeneration on the biomimetic nanostructured matrix," *International Journal of Pharmaceutics,* vol. 463, p. 17, 2014.
[22] A. Paatero *et al.*, "Crystal Structure of an Engineered LRRTM2 Synaptic Adhesion Molecule and a Model for Neurexin Binding," (in English), *Biochemistry,* Article vol. 55, no. 6, pp. 914-926, Feb 2016.
[23] J. de Wit and A. Ghosh, "Specification of synaptic connectivity by cell surface interactions," (in English), *Nature Reviews Neuroscience,* Review vol. 17, no. 1, pp. 22-35, Jan 2016.
[24] P. Scheiffele, J. H. Fan, J. Choih, R. Fetter, and T. Serafini, "Neuroligin expressed in nonneuronal cells triggers presynaptic development in contacting axons," (in English), *Cell,* Article vol. 101, no. 6, pp. 657-669, Jun 2000.
[25] A. M. Craig and Y. Kang, "Neurexin-neuroligin signaling in synapse development," (in English), *Current Opinion in Neurobiology,* Article vol. 17, no. 1, pp. 43-52, Feb 2007.
[26] C. Dean *et al.*, "Neurexin mediates the assembly of presynaptic terminals," (in English), *Nature Neuroscience,* Article vol. 6, no. 7, pp. 708-716, Jul 2003.
[27] J. de Wit *et al.*, "LRRTM2 Interacts with Neurexin1 and Regulates Excitatory Synapse Formation," (in English), *Neuron,* Article vol. 64, no. 6, pp. 799-806, Dec 2009.
[28] M. E. Spira and A. Hai, "Multi-electrode array technologies for neuroscience and cardiology," (in English), *Nature Nanotechnology,* Review vol. 8, no. 2, pp. 83-94, Feb 2013.
[29] P. Fattahi, G. Yang, G. Kim, and M. R. Abidian, "A Review of Organic and Inorganic Biomaterials for Neural Interfaces," *Advanced Materials,* vol. 26, no. 12, pp. 1846-1885, 2014.
[30] C. Mora Lopez *et al.*, "A Neural Probe With Up to 966 Electrodes and Up to 384 Configurable Channels in 0.13 μm SOI CMOS," *IEEE Transactions on Biomedical Circuits and Systems,* vol. 11, no. 3, pp. 510-522.
[31] N. Pour Aryan, *Stimulation and Recording Electrodes for Neural Prostheses* (SpringerBriefs in Electrical and Computer Engineering). Cham: Cham : Springer International Publishing, 2014.
[32] M. Jorfi, J. L. Skousen, C. Weder, and J. R. Capadona, "Progress towards biocompatible intracortical microelectrodes for neural interfacing applications," (in English), *Journal of Neural Engineering,* Review vol. 12, no. 1, p. 45, Feb 2015, Art. no. 011001.
[33] S. F. Cogan, "Neural Stimulation and Recording Electrodes," vol. 10, ed, 2008, pp. 275-309.
[34] M. A. Lebedev and M. A. L. Nicolelis, "Brain-machine interfaces: past, present and future," (in English), *Trends in Neurosciences,* Review vol. 29, no. 9, pp. 536-546, Sep 2006.
[35] D. Prodanov and J. Delbeke, "Mechanical and Biological Interactions of Implants with the Brain and Their Impact on Implant Design," (in English), *Frontiers in Neuroscience,* Review vol. 10, p. 20, Feb 2016, Art. no. 11.
[36] D. Prodanov and J. Delbeke, "Mechanical and Biological Interactions of Implants with the Brain and Their Impact on Implant Design," *Frontiers in Neuroscience,* vol. 10, 2016.

[37] R. Biran, D. C. Martin, and P. A. Tresco, "Neuronal cell loss accompanies the brain tissue response to chronically implanted silicon microelectrode arrays," (in English), *Experimental Neurology,* Article vol. 195, no. 1, pp. 115-126, Sep 2005.
[38] V. S. Polikov, P. A. Tresco, and W. M. Reichert, "Response of brain tissue to chronically implanted neural electrodes," (in English), *Journal of Neuroscience Methods,* Review vol. 148, no. 1, pp. 1-18, Oct 2005.
[39] T. D. Y. Kozai, A. S. Jaquins-Gerstl, A. L. Vazquez, A. C. Michael, and X. T. Cui, "Brain Tissue Responses to Neural Implants Impact Signal Sensitivity and Intervention Strategies," (in English), *Acs Chemical Neuroscience,* Review vol. 6, no. 1, pp. 48-67, Jan 2015.
[40] N. A. Kotov *et al.*, "Nanomaterials for Neural Interfaces," vol. 21, ed. Weinheim, 2009, pp. 3970-4004.
[41] R. Balint, N. J. Cassidy, and S. H. Cartmell, "Conductive polymers: Towards a smart biomaterial for tissue engineering," *Acta Biomaterialia,* vol. 10, no. 6, pp. 2341-2353, Jun 2014.
[42] E. Tamburri, S. Orlanducci, F. Toschi, M. L. Terranova, and D. Passeri, "Growth mechanisms, morphology, and electroactivity of PEDOT layers produced by electrochemical routes in aqueous medium," *Synthetic Metals,* vol. 159, no. 5-6, pp. 406-414, Mar 2009.
[43] D. H. Kim, S. M. Richardson-Burns, J. L. Hendricks, C. Sequera, and D. C. Martin, "Effect of immobilized nerve growth factor on conductive polymers: Electrical properties and cellular response," *Advanced Functional Materials,* vol. 17, no. 1, pp. 79-86, Jan 2007.
[44] A. G. Rylie, "ORGANIC ELECTRODE COATINGS FOR NEXT- GENERATION NEURAL INTERFACES," *Frontiers in Neuroengineering,* vol. 7, no. NA, pp. NA-NA.
[45] S. Patra, K. Barai, and N. Munichandraiah, "Scanning electron microscopy studies of PEDOT prepared by various electrochemical routes," (in English), *Synthetic Metals,* Article vol. 158, no. 10, pp. 430-435, Jun 2008.
[46] G. L. M. Cheong, K. S. Lim, A. Jakubowicz, P. J. Martens, L. A. Poole-Warren, and R. A. Green, "Conductive hydrogels with tailored bioactivity for implantable electrode coatings," (in English), *Acta Biomaterialia,* Article vol. 10, no. 3, pp. 1216-1226, Mar 2014.
[47] S. Kalia, *Polymeric Hydrogels as Smart Biomaterials*, 1st ed. 2016. ed. (Springer Series on Polymer and Composite Materials). Cham: Cham : Springer International Publishing : Imprint Springer, 2016.
[48] A. Kumar and S. S. Han, "PVA-based hydrogels for tissue engineering: A review," (in English), *International Journal of Polymeric Materials and Polymeric Biomaterials,* Review vol. 66, no. 4, pp. 159-182, 2017.
[49] J. M. Coburn, M. Gibson, S. Monagle, Z. Patterson, and J. H. Elisseeff, "Bioinspired nanofibers support chondrogenesis for articular cartilage repair," (in English), *Proceedings of the National Academy of Sciences of the United States of America,* Article vol. 109, no. 25, pp. 10012-10017, Jun 2012.
[50] P. N. Shah *et al.*, "Environmentally benign synthesis of vinyl ester resin from biowaste glycerin," *RSC Advances,* vol. 5, no. 48, pp. 38673-38679.
[51] K. S. Lim, M. H. Alves, L. A. Poole-Warren, and P. J. Martens, "Covalent incorporation of non- chemically modified gelatin into degradable PVA-tyramine hydrogels," *Biomaterials,* vol. 34, no. 29, pp. 7097-7105.
[52] A. J. Patton, R. A. Green, and L. A. Poole-Warren, "Mediating conducting polymer growth within hydrogels by controlling nucleation," *Apl Materials,* vol. 3, no. 1, Jan 2015, Art. no. 014912.

[53] R. A. Green *et al.*, "Conductive Hydrogels: Mechanically Robust Hybrids for Use as Biomaterials," (in English), *Macromolecular Bioscience,* Article vol. 12, no. 4, pp. 494-501, Apr 2012.
[54] J. Goding, A. Gilmour, P. Martens, L. Poole-Warren, and R. Green, "Interpenetrating Conducting Hydrogel Materials for Neural Interfacing Electrodes," *Advanced Healthcare Materials,* p. <xocs:firstpage xmlns:xocs=""/>.
[55] D. S. W. Benoit and K. S. Anseth, "Heparin functionalized PEG gels that modulate protein adsorption for hMSC adhesion and differentiation," (in English), *Acta Biomaterialia,* Article vol. 1, no. 4, pp. 461-470, Jul 2005.
[56] C. H. Thompson, M. J. Zoratti, N. B. Langhals, and E. K. Purcell, "Regenerative Electrode Interfaces for Neural Prostheses," (in English), *Tissue Engineering Part B-Reviews,* Review vol. 22, no. 2, pp. 125-135, Apr 2016.
[57] E. Bieberich and A. Guiseppi-Elie, "Neuronal differentiation and synapse formation of PC12 and embryonic stem cells on interdigitated microelectrode arrays: Contact structures for neuron-to-electrode signal transmission (NEST)," *Biosensors & Bioelectronics,* vol. 19, no. 8, pp. 923-931, Mar 2004.
[58] S. B. Jun *et al.*, "Low-density neuronal networks cultured using patterned poly-L-lysine on microelectrode arrays," (in English), *Journal of Neuroscience Methods,* Article vol. 160, no. 2, pp. 317-326, Mar 2007.
[59] K. Czondor *et al.*, "Micropatterned substrates coated with neuronal adhesion molecules for high-content study of synapse formation," (in English), *Nature Communications,* Article vol. 4, p. 14, Aug 2013, Art. no. 2252.
[60] K. Eun Joong, J. Chang Su, L. Soo Youn, H. Inseong, and C. Taek Dong, "Robust Type-specific Hemisynapses Induced by Artificial Dendrites," *Scientific Reports,* vol. 6.
[61] M. Inc., "Streptavidin surfaces," ed. http://www.proteinslides.com/streptavidin, 2010.
[62] C. R. Nuttelman, D. J. Mortisen, S. M. Henry, and K. S. Anseth, "Attachment of fibronectin to poly(vinyl alcohol) hydrogels promotes NIH3T3 cell adhesion, proliferation, and migration," (in English), *Journal of Biomedical Materials Research,* Article vol. 57, no. 2, pp. 217-223, Nov 2001.
[63] T. scientific, "carbodiimide crosslinker chemistry," ed: https://www.thermofisher.com/be/en/home/life-science/protein-biology/protein-biology-learning-center/protein-biology-resource-library/pierce-protein-methods/carbodiimide-crosslinker-chemistry.html, 2017.
[64] D. T. Simon *et al.*, "Organic electronics for precise delivery of neurotransmitters to modulate mammalian sensory function," (in English), *Nature Materials,* Article vol. 8, no. 9, pp. 742-746, Sep 2009.

Master's Thesis file

Students: Jasper Timmerman

Title: Synaptoprobe: interfacing at the synapse level

English title: Synaptoprobe: interfacing at the synapse level

Content in brief: (maximum 500 words)

The field of brain machine interfacing and neuroscience in general is rapidly expanding. Exciting new technologies are being developed for the near future. To expedite the developments in neuroscience and brain machine interfacing the development of a novel concept probe is explored. The synaptoprobe is designed to make specific connections with targeted subpopulations of neurons. Conceptually the synaptoprobe would utilize the unique properties of synaptogenic proteins immobilized onto electrode surfaces. In the approach described here, a conductive hydrogel is deposited onto electrodes as a scaffold for synaptogenic proteins neuroligin 1 and LRRTM 2, while maintaining low impedance and improving biocompatibility. The synthesis of the hydrogel was achieved, and two different pathways to immobilize neuroligin 1 and LRRTM 2 were developed.

Thesis submitted to obtain the degree of Master in Engineering: Nanoscience and nanotechnology; specializing in nanobiotechnology

Supervisor(s): Professor Marc Heyns, Professor Sebastian Haesler, Professor Jennifer Patterson
Assessors: Professor Joris De Wit, Luis Hoffman
Mentor(s): Luis Hoffman